

Submitted to the special issue dedicated to Michel Boudart

Experimental and Computational Kinetics Study of the Liquid-phase Hydrogenation of C=C and C=O Bonds

Gengnan Li,[#] Zheng Zhao,[#] Tong Mou, Qiaohua Tan, Bin Wang, Daniel Resasco*

School of Chemical, Biological and Materials Engineering,
University of Oklahoma, Norman, OK 73019, USA

[#] These authors contributed equally

* Corresponding author. Email address: resasco@ou.edu

Abstract

Solvent effects on adsorption equilibrium and reaction kinetics are evaluated for hydrogenation reactions catalyzed by Pd/alumina in a series of different solvents. Three reactants – cyclohexene, benzene and benzaldehyde – and three solvents – n-heptane (HEP), methylcyclohexane (MCHA), decalin (DL) – have been investigated. Kinetic analysis of hydrogenation of cyclohexene reveals that hydrogen adsorbs on different sites from those where cyclohexene and the solvents adsorb; however, the presence of hydrogen on these separate sites affects the heats of adsorption of the hydrocarbons. When the solvent is a weakly interacting linear alkane (HEP), the rate determining step of the reaction is the first hydrogenation of adsorbed cyclohexene. This conclusion is supported by DFT calculations that show a higher enthalpy barrier for the first hydrogenation than for the second, while statistical thermodynamics analysis validates the physical significance of the entropy of adsorption parameters derived from the kinetic fitting of experimental data. By contrast, with solvents such as MCHA and DL, which interact more strongly with the metal surface and compete for active sites with the reactant and the surface intermediate, the rate limiting step seems to shift to the second hydrogenation step.

One of the main conclusions of the study is that the effects observed with non-polar solvents are mostly due to competitive adsorption of the solvent, which causes a decrease in surface coverage of reactants and surface intermediates. Indeed, under identical conditions, the hydrogenation rates of C=C bonds in cyclohexene (or the aromatic ring in benzene) follow the order HEP>MCHA>DL, which is consistent with the strongest solvent/metal interaction for DL and the weakest for HEP. Further, binary solvent mixtures of DL-HEP exhibit non-idealities that are clearly evident in the fitting of hydrogenation rates. It is proposed that the higher activity coefficient of liquid DL in the liquid mixture enhances its surface coverage, competing more effectively with the reactant, which causes a decrease in catalytic activity larger than that predicted assuming an ideal mixture of solvents.

Likewise, large drops in benzene hydrogenation rates are observed in water-organic co-solvent mixtures due to the competitive adsorption of water on the Pd surface. It is proposed that water adsorption is further enhanced by the non-ideality of the water-organic mixture. By contrast, in the hydrogenation of the C=O bond of benzaldehyde, the presence of water provides a favorable alternative reaction path with lower activation barrier, which results in higher hydrogenation activity when the reactant is a carbonyl-containing molecule, such as benzaldehyde. In this system, the H-bonded water network assists shuttling a proton from the Pd surface to the hydrophilic O atom in C=O, assisted by surface charge separation. Since this H transfer pathway cannot take place with C=C bonds or aromatic rings, only site inhibition occurs for these reactions.

Keywords: solvent effect; kinetics; non-ideal solution; competitive adsorption; proton transfer

1. Introduction

The different potential effects of solvents in liquid-phase reactions and the complexities that they bring to the analysis of reaction kinetics was a topic of great interest to Michel Boudart [1, 2]. He reminded us that the reacting liquid mixture may not necessarily be ideal and, consequently, these thermodynamic non-idealities should be contemplated in the reaction kinetics treatment [3, 4]. That is, while in ideal systems the kinetic and thermodynamic parameters included in the rate laws are expressed in terms of concentrations, in non-ideal systems thermodynamic activities and fugacities should be used. In these cases, the choice of solvent can have a significant effect on observed rates. Boudart also emphasized the value of combining computational chemistry with kinetic analysis in a combinatorial iteration that can lead to the development of optimized catalysts [5]. Appropriately, in this contribution, we study ideal and non-ideal systems, combining experimental kinetics with partition function and density functional theory (DFT) calculations to obtain kinetic and thermodynamic parameters that describe the hydrogenation of C=C and C=O bonds in the liquid-phase.

Solvents are ubiquitous in liquid-phase reactions, and they are usually selected based on their ability to solubilize the reactants and products, or their heat transfer properties [6, 7]. However, they can also provide additional degrees of freedom to facilitate combined reaction/separation strategies based on relative solubilities that might result in significant techno-economic advantages [8-12]. Perhaps, the most widely investigated solvent effects are those that cause changes in reaction activity and selectivity, which are typically linked to solvent polarity and its resulting solvent-reactant, solvent-catalyst or solvent-solvent interactions [13-15]. The associated thermodynamic non-idealities have been considered in several studies [3, 4, 16, 17]. A now classical example for the application of non-ideal thermodynamic formalisms in the reaction rate expressions is that proposed by Boudart and co-workers [1, 2] when analyzing the kinetics of liquid-phase cyclohexene hydrogenation on various metal catalysts, with a wide range of solvents. They found that the effect of H₂ solubility (concentration) on cyclohexene hydrogenation rate depends on the nature of the metal. On Pt catalysts, the turnover frequency (TOF) of cyclohexene hydrogenation increased with the H₂ solubility of the solvent. By contrast, on Pd catalyst, TOF stayed relatively constant in non-aromatic solvents, regardless of changes in H₂ solubility. They further proposed that the different catalytic behaviors depended on whether or not the initial and transition states at the rate-determining step (RDS) are solvated to same extent by the solvent [3]. That is, they suggested that on the Pt catalyst, the solvation effect on dissolved H₂ in the initial state and in the activated complexes of the transition states are identical, leading to a fortuitous cancellation of the activity coefficients, leaving the concentration of dissolved H₂ as the critical parameter in the rate expression [3]. Only in this case, the hydrogenation rate is proportional to H₂ solubility. By contrast, they inferred that solvation must play a much less significant role in initial and transition states over Pd, on which adsorption of cyclohexene and hydrogen was considered to occur on separate sites [2, 18]. The adsorbed H and cyclohexene in the RDS are influenced by strong interaction with Pd surface, which suppresses the effect of solvation by the surrounding solvent molecules. Therefore, it was concluded that the hydrogenation rate on Pd is less affected

by the identity of the solvent than that on Pt. These observations demonstrate that reaction rates in non-ideal solutions are determined by thermodynamic properties rather than concentrations [1, 4, 18, 19].

An alternative to the use of activity coefficients instead of concentrations in the rate expression is to treat the non-ideality in terms of an excess free energy, which can be incorporated in the apparent free energy of activation [20]. Consequently, the temperature-independent excess entropy can be taken as a modifier of the concentration term, converting the non-ideality effects in the reaction rate into entropic effects of the solvent on the transition state relative to the reactant in the liquid phase. In fact, Bregante et al. [21] have found that the unfavorable interactions between the hydrophobic aliphatic chain of 1-octane in the epoxidation transition state and the water clusters near a silanol group within Ti-Beta zeolite lead to the reorganization of the H-bonded network, which increases the entropy of the water clusters. As a result, by increasing the density of silanol groups and consequently hydrophilicity of the zeolite, a larger transition state entropy is achieved, which reduces the net free energy and thereby increases the rate of epoxidation.

Likewise, Schwartz et al. [22] have applied the transition-state theory (TST) formalism to a biphasic reaction system and proposed that when the interphase mass transfer is infinitely fast and the solvent does exchange between the phases, the enhancement of selectivity in biphasic system is mainly caused by the solvation of the stable species. They have also shown that polymers can modify the surface properties of metal catalysts by acting as a local pseudo-solvent and solvating species bound to the metal surface [23]; in this case, considering the non-ideality of the reaction system, the authors suggested that the microenvironment influences the reaction rate both by altering the surface coverage of the reactant and by solvating the transition state of the RDS to a different extent than the reactant, which affects the activation energy.

In addition to non-idealities, other effects such as competitive adsorption by the solvent on relevant sites [14, 24, 25], changes in intrinsic kinetics [26-28], or even direct participation of the solvent in the reaction pathway [9, 29-31] should be considered. For example, an energy compensation between adsorbed reactants and displaced solvent molecules has been suggested for the adsorption step occurring during reaction. To accurately evaluate solvent effects on the adsorption of a given reactant, Campbell and coworkers [32, 33] compared the adsorption energies of the reactant on a solid from a solvent to that from the gas phase. By combining a thermodynamic cycle with a pairwise bond-additivity model they found that the heat of adsorption of reactant (reactant-solid interaction) from the liquid phase is compensated by the energy cost to break the solvent-solid interface, and thus a lower net adsorption energy is observed in liquid than in vacuum. Complementing this study, classical molecular dynamics (MD) simulations based on an accurate many-body force field [34] showed that the difference in adsorption free energies of a molecule could be attributed to differences in both enthalpy and entropy changes. In vacuum, the adsorption of the molecule on the catalyst surface leads to a significant loss in its degrees of freedom (negative entropy change), which makes the free energy changes less favorable for adsorption, but this is compensated by the highly exothermic enthalpy change. By contrast, the liquid phase systems have a less exothermic enthalpy change, but at the same time, the entropy losses of adsorbed

molecules are less significant because they are compensated by the entropy gains of the desorbed solvent molecules displaced from the surface by the solute.

Collectively, these studies demonstrate that the presence of a solvent may modify the structure of the adsorbed reactants, intermediates, and reaction transition states, which cause changes in the enthalpy and entropy of activation of the surface reaction. Thus, differences in rates, selectivities, and kinetic parameters are expected when varying the solvent. Generally, reactants with high affinity for the solvent result in ideal systems with activity coefficients close to unity [18]. On the contrary, low affinity between the solvent and the reactant due to different polarities produce a higher degree of thermodynamic non-ideality. In these mixtures, the solvent may repel the reactant towards the catalyst surface, increasing the surface coverage of the adsorbed species at a given concentration of the bulk phase [18]. At the same time, a strong solvent-surface interaction may drive the solvent molecule to compete for adsorption sites, lowering the reactant surface coverage. Since reaction rates are a function of the total number of adsorbed reacting species, a modified surface coverage of reactants by solvent co-adsorption should influence reaction rates. For example, Wan et al. [35] performed a systematic study of solvents effects in the hydrogenation of oxygenates on a Ru/C catalyst. They found that the rate of 2-butanone hydrogenation in different solvents follows the order of solvent used: polar protic > non-polar aprotic > polar aprotic. In protic solvents (e.g. water and alcohol), the strong interaction between the solvent and an oxygenate reactant lowers the activation energy barrier via a proton shuttle mechanism through the H-bonded network of the solvent. Therefore, the absence of a H-bonded network in aprotic solvents leads to lower hydrogenation rates. Finally, in polar aprotic solvents, strong solvent-catalyst interactions also lead to low hydrogenation rates due to the competitive adsorption of the solvent on active sites. By contrast, neither solvent-reactant nor solvent-catalyst interaction is significant in non-polar aprotic solvents; this lack of interaction results in a moderate hydrogenation rate of oxygenates in hydrocarbon solvents.

Solvents can assist or inhibit reaction rates by tuning the composition of surface species and/or by directly participating in the reaction pathway [9, 29-31]. The observed solvent effects can be interpreted by the thermodynamic properties of the reaction mixture such as non-ideality, entropy compensation between adsorbed species and displaced solvent molecule, and compensation effect between enthalpy and entropy in adsorption and transition state. Therefore, it is clear that, to get a complete and quantitative picture of reactions in liquid phase a coherent combination of computational simulations and careful experimental measurements (free of parasitic phenomena) is required [36]. An accurate kinetic model that incorporates solvent effects in the rate equations not only should describe the experimental phenomena mathematically, but also provide valuable validation for computational calculations [37-39]. Consequently, thermodynamic properties such as entropy and enthalpy changes during adsorption and reaction can be interpreted.

In this work, several kinetic models incorporating solvent terms, coupled with statistic calculations and DFT modeling have been applied to investigate the role of non-idealities in different solvents for the Pd-catalyzed hydrogenation of C=C and C=O bonds in nonpolar and

polar solvents, as well as their mixtures. Kinetic analysis over the entire range of surface coverages reveals that the observed differences in C=C hydrogenation rates when varying the solvent is mainly caused by the different extents of competitive adsorption of solvent molecules [2, 18]. It is proposed that when a polar reactant (C=O) is used, a non-polar solvent repels the polar reactant from the bulk, causing stronger adsorption on the catalyst surface, leading to higher coverage of the reactant. As a result, solvent effects are insignificant in C=O hydrogenation reactions with non-polar solvents.

We have also investigated non-idealities in the hydrogenation of C=C and C=O bonds in polar-nonpolar (water-organic) co-solvent systems. While competitive adsorption of water leads to decreased hydrogenation rates in C=C hydrogenation, the presence of water provides an additional reaction pathway for the C=O hydrogenation with lower activation barrier by forming H-bonded network, which is absent in the C=C bond hydrogenation due to the non-polar nature of the C atom.

2. Experimental

2.1 Catalyst preparation. The Pd/ α -Al₂O₃ catalyst used in this study was synthesized by conventional incipient wetness impregnation, with 0.25 or 1.0 wt.% Pd loading. Low surface area, non-porous α -Al₂O₃ was used as a support to minimize parasitic phenomena such as metal-support interactions and internal mass transfer limitations; accordingly, the focus of the study is placed on the kinetic behavior and solvent effects rather than on the catalyst itself. An aqueous solution of palladium(II) nitrate dihydrate (Sigma-Aldrich) precursor was added drop by drop onto the catalyst support α -Al₂O₃ (Sigma-Aldrich); the resulting solid was first dried overnight at 70°C and then calcined in air for 6 h at 300°C.

2.2 Catalyst Characterization. The catalysts were characterized in a transmission electron microscope JEOL JEM-2100, equipped with a LaB₆ gun and operated at an accelerating voltage of 200 kV. The TEM sample was prepared by drop-casting a sonicated propanol suspension containing the pre-reduced Pd/ α -Al₂O₃ sample onto a holey carbon film mounted on a copper TEM grid. The Pd particles were analyzed using ImageJ to acquire particle size distribution and surface structure. TEM images of 0.25 wt.% Pd/ α -Al₂O₃ are shown in **Figure S1** (Supplementary material). It is observed that the metallic Pd particles are homogeneously dispersed on the α -Al₂O₃ support. The surface-weighted average diameter estimated from over hundreds of Pd particles is 3.13 nm, corresponding to a Pd dispersion of about 36 % [40]. HRTEM indicates that the Pd cluster surfaces on the 0.25 wt.% Pd/ α -Al₂O₃ were mostly composed of (111) planes. Therefore, in the theoretical calculations we have utilized closed-packed Pd (111) surfaces to model the catalyst. Uniform dispersion of the Pd particles on the α -Al₂O₃ surface was also demonstrated for the 1 wt% Pd/ α -Al₂O₃ catalyst by HRTEM analysis, as shown in **Figure S2**. The average diameter of Pd estimated from over hundreds of Pd nanoparticles is 3.45 nm, corresponding to a Pd dispersion of about 30 %.

2.3 Catalytic reactions. The liquid-phase catalytic hydrogenation of cyclohexene was carried out in a 300 mL high temperature/high pressure Parr batch reactor, equipped with an IR probe (Mettler Toledo ReactIR iC 10) for in-situ measurements that allowed a continuous monitoring of cyclohexene concentration as a function of reaction time [41]. As shown in **Figure S3** and **S4** in supplementary material, reaction rates were measured under kinetic regime, meticulously excluding external or internal mass transport limitation and deactivation effects. In a steady-state flow reactor, determining k_D is rather straightforward as one can measure variation of steady-state rates as a function of time. However, evaluating deactivation in a batch reactor is much more complicated since the concentrations continuously change at a rate that depends on both reaction kinetics and deactivation. An effective method for decoupling deactivation and kinetics in a batch reactor has been described by Apesteguía et al. [42, 43]. In this method, the evolution of reactant concentration is plotted as a function of the product of catalyst mass and time ($m \cdot t$) for two different amounts of catalyst. Regardless of the kinetics, the drop in concentration is a function of kt (for instance $C/C_0 = e^{-kt}$ for first order; or $C_0 - C = kt$ for zeroth order). The rate constant $k = m \cdot k_i$, with m = catalyst mass and k_i = specific rate constant per gram. When we use the product ($m \cdot t$) as a variable and k_i remains constant with time, curves of C vs. ($m \cdot t$) are superimposed for different catalyst masses because the time needed to reach a certain conversion is inversely proportional to m and k_i is constant. However, if there is deactivation and k_i is not constant with time the curves depart from each other since, with a smaller mass, a longer time is required to reach a given conversion and so the catalyst experiences more pronounced deactivation than in a run with a larger amount of catalyst and shorter time. The more separated are the curves with different catalyst amounts, the stronger is the extent of deactivation. In our case, the results of this test showed that the deactivation during the first 30 min is essentially negligible (see Supplementary Material Fig. S3).

The IR probe allows for continuous in-situ quantification of liquid phase cyclohexene concentration during hydrogenation. Before the reactant injection, the probe was scanned in the solvent to obtain the background that was later subtracted from the actual run spectrum. When the reactant feed was purged in the vessel, the reaction started. A scan was taken every minute. The characteristic IR absorption frequencies of 1139 cm^{-1} (ωCH_2 rock) and 719 cm^{-1} (C-H out-of-plane bending) [44] on the acquired IR spectrum were utilized for quantifications since these bands that only appear for cyclohexene, which allows for a precise determination of cyclohexene concentration as a function of time. From this plot, the hydrogenation reaction rate was obtained by measuring the slope of the reaction IR profile at each moment.

The non-polar aprotic inert solvents used in the study were n-heptane (Sigma-Aldrich, anhydrous, 99%), methylcyclohexane (Sigma-Aldrich, anhydrous, $\geq 99\%$), and decalin (Sigma-Aldrich, anhydrous, $\geq 99\%$). The reactant cyclohexene (Sigma-Aldrich, with BHT as inhibitor, $\geq 99\%$) was first distilled in N_2 flow at 50°C to eliminate the inhibitor BHT. The distilled cyclohexene was then filtered through a column packed with $\gamma\text{-Al}_2\text{O}_3$ (Alfa Aesar) to remove the trace amounts of other impurities that may cause catalyst deactivation during reaction. The purified

cyclohexene was stored in a freezer when not being used. These precautions are necessary to avoid any irreproducibility in the reaction measurements.

A given amount of catalyst 0.25 wt.% Pd/ α -Al₂O₃ and 100 mL solvent were charged into the reactor vessel. The catalyst was reduced in flowing H₂ at 100°C for an hour, which is enough to fully reduce Pd [45]. A 20 mL volume of cyclohexene reactant was pressurized in the reactor vessel to the desired injection pressure at the reaction temperature ranging from 40°C to 100°C. The reaction pressure was varied widely from 2.4 atm to 61 atm. For runs with binary solvent mixtures, the secondary solvent was added along with the primary solvent and the catalyst before the reduction step.

The liquid-phase catalytic reactions of benzene (Sigma-Aldrich, anhydrous, 99.8 %) and benzaldehyde (Sigma-Aldrich, redistillation, ≥ 99.5 %) hydrogenation reactions were carried out in the 300 mL high temperature and high-pressure Parr batch reactor. For example, 50 mg catalyst 1.0 wt.% Pd/ α -Al₂O₃ was mixed with 80 mL solvent, followed by reduction in 6.8 atm hydrogen at 100 °C for one hour. Then the reactor was cooled down to 70 °C for the reaction. Reactant, benzene or benzaldehyde, was introduced to the reactor vessel along with solvent by pressurizing the feed cylinder. The final total liquid volume was 100 mL, and reaction pressure was 41 atm H₂. For the reaction conducted with the presence of water, 1.0 mL water was added along with the catalyst and solvent at the beginning of the reduction. The concentrations of benzene and benzaldehyde are 0.2 mol/L.

After reaction, the reactor was cooled down to room temperature and liquid was separated from mixture by filtration. Finally, the liquid phase was analyzed on a 7890B Agilent GC-FID equipped with ZB-5 and ZB-WAX GC columns. For cyclohexene hydrogenation, the conversion calculated from IR measurements was corroborated by GC-FID, along with carbon balance calculations, which was > 99% in all cases. Conversion is defined by the following equation:

$$\text{Conversion } x\% = \frac{\text{mole of reactant reacted}}{\text{mole of reactant charged}} \times 100\% \quad (1)$$

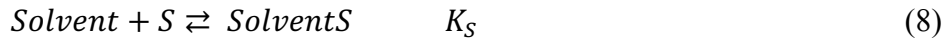
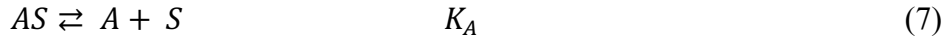
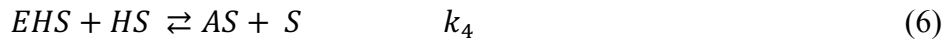
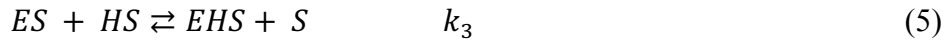
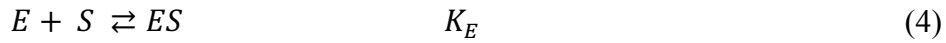
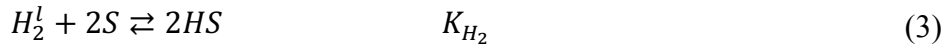
2.4 DFT calculations. Density functional theory calculations were carried out using the Vienna Ab initio simulation package (VASP) [46]. The Perdew-Burke-Ernzerhof generalized gradient approximation exchange-correlation potential (PBE-GGA) was used [47], and the electron-core interactions were treated in the projector augmented wave (PAW) method [48]. Van der Waals interactions have been taken into account using the Grimme's DFT-D3 semiempirical method [49, 50]. The reactions were modeled accordingly. Structures were optimized with a kinetic cutoff energy of 400 eV relaxed until the force acting on each atom is smaller than 0.02 eV Å⁻¹. The Pd(111) metal surface was modeled with a 4 × 4 unit cell with four atomic layers. Similarly, H-terminated PdH surface was also modeled using a four layer 4 × 4 surface slab, with bottom two layers frozen to reflect the bulk. Computed bulk lattice constants are 3.885 and 4.075 Å for Pd and PdH. The vacuum between the slabs was set at 20 Å to minimize the effect of the interaction between them. The Brillouin zone was sampled with a 3 × 3 × 1 k-point grid.

Transition state searches were performed using the dimer method [51] with the initial guesses for the transition state structure obtained through the nudged elastic band (NEB) method[52]. The transition states were confirmed with the presence of a unique imaginary frequency in vibration frequency calculations. The adsorption energy was calculated as $E_{\text{ads}} = (E_{\text{ni/slab}} - E_{\text{slab}} - nE_i) / n_i$ where $E_{\text{ni/slab}}$, E_{slab} , and E_i are the total electronic energy of adsorbate/slab system, clean metal slab, and the isolated adsorbate in gas phase, respectively, and n is the number of adsorbates on the metal slab.

3. Results and discussion

3.1. Comparison of kinetic models to describe the cyclohexene hydrogenation reaction at constant temperature ($T = 70^\circ \text{C}$)

Following Boudart's pioneering studies [2] on cyclohexene hydrogenation, we have considered the following sequence of elementary steps:



where H stands for hydrogen, E for cyclohexene, EH for the partially hydrogenated cyclohexene surface intermediate, A for cyclohexane, and S for surface sites.

Two types of models can be considered, depending on whether all species compete for the same type of sites [25] or not. In the first case, the site balance would be:

$$1 = \theta_v + \theta_{HS} + \theta_{ES} + \theta_{EHS} + \theta_{AS} + \theta_{\text{Solvent}S} \quad (9)$$

Previous studies on Pd (111) have suggested that the much smaller H atom preferentially adsorbs on the three-fold fcc sites [53] without competing with larger adsorbed species and solvents, which adsorb on top sites [53-56]. In that case, reacting species and solvent are considered to adsorb on the same type of site, but H on different sites [57-59]; that is:

$$1 = \theta_{v1} + \theta_{HS1} \quad (10)$$

$$1 = \theta_{v2} + \theta_{ES2} + \theta_{EHS2} + \theta_{AS2} + \theta_{\text{Solvent}S2} \quad (11)$$

Since the dissociation of H_2 has a very low barrier on the Pd surface, it cannot be RDS [60]. Herein, we only contemplate addition of H to a surface species as RDS; so, four possible kinetic models can be considered depending on whether the first or second hydrogenation is rate limiting, and whether H is absorbed on the same or on different sites from the other surface species.

To consider thermodynamic non-idealities the adsorption equilibrium constants should be expressed in terms of thermodynamic activities, which take into account the solvent-solute and solvent-solvent interactions that may affect the surface coverage of species, and consequently, the rates [61]. Since concentrations of reactants, products, and solvents are measured in the liquid phase, the rate expressions are described in terms of $a_i = \gamma_i C_i$, which may change from solvent to solvent. On the other hand, H_2 partial pressures are measured in the gas phase, which are considered in pseudo-equilibrium with the surface, regardless of the solvent used. Therefore, the rate expressions are described in terms of P_{H_2} . By definition, the adsorption constants $K_i = e^{-\Delta G_i/RT}$; therefore, they have no units. In the liquid phase $K_i = \Pi a_i^{v_i}$, where the thermodynamic activities are expressed in measured concentrations relative to a standard state, which for convenience is taken as 1 M. Therefore, the units of concentration cancel out when they are expressed as mol/L, which in the ideal case, makes K the same numerical value as using concentrations, but without units. Of course, in non-ideal systems, concentration must be multiplied by γ_i , but again, units cancel out. Similarly, for gases, the standard state is chosen as 1 atm, so K has no units and P_i must be expressed in atmospheres [62].

The activity coefficients at infinite solute dilution obtained from the UNIQUAC estimations in ASPEN Plus are listed in **Table 1**. For the binary mixtures of solvents, the values of activity coefficient at each co-solvent composition were derived by ASPEN Plus.

Table 1. Activity coefficients of reactants and solvents at infinite dilution.

Solute	Solvent		
	heptane HEP	methylcyclohexane MCHA	decalin DL
heptane	1.00	1.02	1.82
methylcyclohexane	1.04	1.00	1.02
decalin	1.52	1.03	1.00
cyclohexene	1.06	1.02	0.97
benzene	1.36	1.32	1.07
benzaldehyde	8.40	7.74	5.13

Cyclohexene displays ideal mixture behavior in all three solvents at all concentrations with activity coefficients $\gamma_E \approx 1$, even at infinite dilution. The solvent binary mixtures also show ideal behavior except for the HEP-DL mixture, for which using the non-ideal parameters obtained with ASPEN Plus at every composition of the binary mixture resulted in a significantly better description of the experimental results (see **Figure 7** and appropriate discussion in section 3.3).

The four kinetic models of non-ideal liquid-phase cyclohexene hydrogenation are listed in **Table 2**. The expressions are written in terms of thermodynamic activities. However, in the case of single non-polar solvent, cyclohexene displays ideal mixture behavior at all concentrations ($\gamma_E \approx 1$), even at infinite dilution. Therefore, in this section, we use liquid phase concentrations in the rate expressions. The expected apparent reaction orders with respect to H_2 pressure (2.4 – 61

atm) and cyclohexene (0 – 3 mol/L) concentrations are analyzed at low and high partial pressures of H₂ and cyclohexene concentrations. For example, in the first model, H₂ adsorbs on the same type of sites as cyclohexene and the solvent, with the first hydrogenation step being rate determining. So, at very low H₂ partial pressures, the H₂ adsorption term $\sqrt{P_{H_2}K_{H_2}}$ in the denominator becomes negligible compared to other adsorption terms, making the rate to be half order with respect to H₂. At high H₂ pressures (P_{H_2}), the H₂ adsorption term becomes dominant, so other adsorption terms become negligible. Consequently, the order with respect to H₂ becomes negative. The same analysis can be applied with respect to the cyclohexene activity (a_E) to determine the expected reaction orders in each case. Making analogous considerations for each of the four models, we obtain the expected reaction orders at low/high values of P_{H_2} and a_E .

Table 2. Kinetic models with corresponding rate expressions and expected reaction orders at limiting conditions ($a_i = \gamma_i C_i$; $\gamma_E \approx 1$).

Model	H ₂ adsorption site	RDS	Rate expression	Reaction order			
				Low P _{H2}	High P _{H2}	Low a _E	High a _E
1	same site	1 st H	$r = \frac{k_3 K_E a_E \sqrt{P_{H_2} K_{H_2}}}{(1 + \sqrt{P_{H_2} K_{H_2}} + K_S a_S + K_E a_E)^2}$	0.5	-0.5	1	-1
2	same site	2 nd H	$r = \frac{k_4 K_{EH} K_E a_E (P_{H_2} K_{H_2})}{(1 + K_E a_E + K_S a_S + \sqrt{P_{H_2} K_{H_2}} + K_{EH} K_E a_E \sqrt{P_{H_2} K_{H_2}})^2}$	1	0	1	-1
3	different site	1 st H	$r = \frac{k_3 K_E a_E \sqrt{P_{H_2} K_{H_2}}}{(1 + K_E a_E + K_S a_S)(1 + \sqrt{P_{H_2} K_{H_2}})}$	0.5	0	1	0
4	different site	2 nd H	$r = \frac{k_4 K_{EH} K_E a_E (P_{H_2} K_{H_2})}{(1 + K_E a_E + K_S a_S + K_{EH} K_E a_E \sqrt{P_{H_2} K_{H_2}})(1 + \sqrt{P_{H_2} K_{H_2}})}$	1	0	1	0

To decide which one of the models gives the best description of the experimental behavior, the reaction was conducted in three different solvents under wide ranges of H₂ pressures and cyclohexene activities.

Figure 1 shows that, at low pressures, the hydrogenation rate increases with H₂ pressure. When the pressure of H₂ is above ~ 20 atm, a plateau is approached in all three solvents. Interestingly, the observed maximum rates are widely different for each solvent. That is, the rate in HEP solvent is twice as that observed in MCHA and almost ten times higher than that in DL. Moreover, the asymptotic approach to zeroth order behavior in H₂ observed at high pressures for all solvents eliminates Model 1, which predicts a negative order at high pressures.

As shown in **Figure 2**, the rate initially increases in all three solvents as cyclohexene concentration increases. Above about 1M, further increase in concentration shows that the rate begins plateauing, without any indication of decreasing, which would be predicted by Models 1 and 2 that show negative reaction orders at high cyclohexene concentrations.

From this analysis, it is clear that H adsorption does not occur on the same type of sites as the reactant and solvents. Therefore, we focus our attention on Models 3 and 4. To choose the one that best describes the observed experimental behavior, we consider the very different rates resulting from runs in the different solvents. The highest rate was obtained with the solvent that more weakly interacts with a metal (HEP) while the lowest rate occurred with the one that interacts most strongly (DL). Hence, the simplest explanation to this solvent effect is competitive adsorption on the same type of sites.

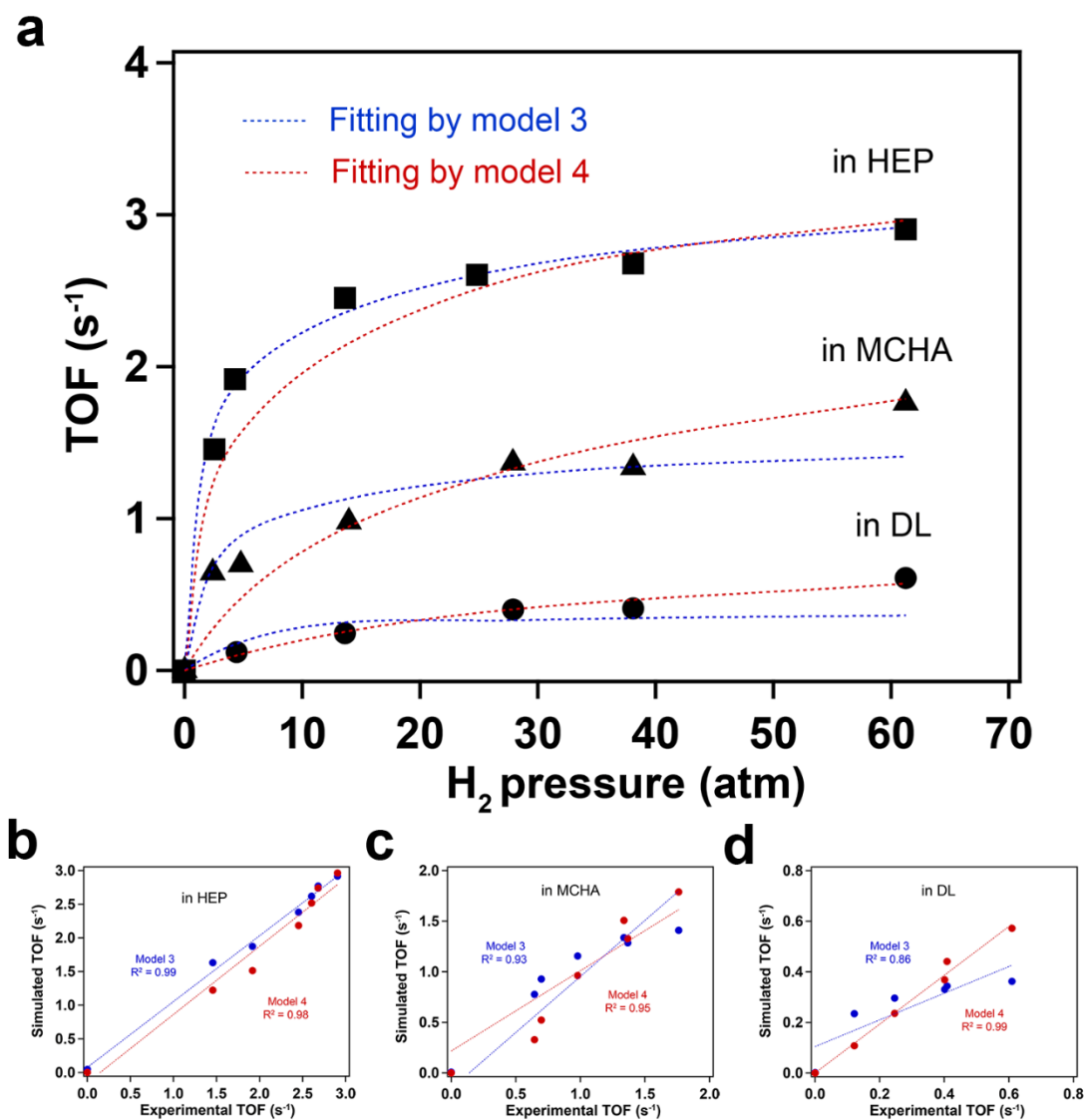


Figure 1. Experimental data of cyclohexene hydrogenation in three different solvents (HEP, MCHA, DL) as a function of H₂ pressure at 70 °C, fitted with Model 3 and Model 4. **(a)** Turnover frequencies (TOF) as a function of H₂ pressure at constant cyclohexene initial concentration of 0.42M. **(b)** Comparison between turnover frequencies (TOF) obtained from experimental measurements. The fittings were done simultaneously for both sets of data, those of this figure and those of Fig.2.

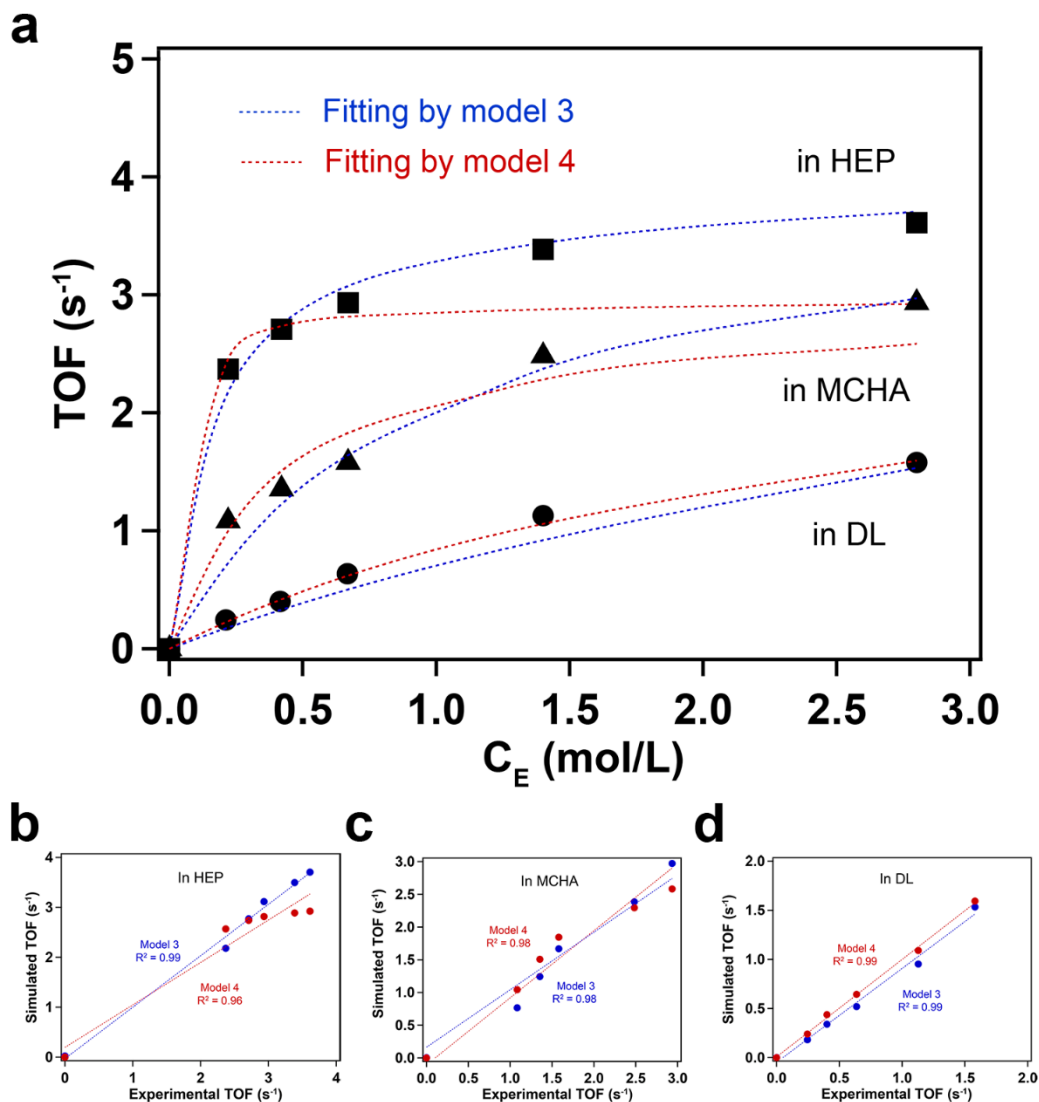


Figure 2. Experimental data of cyclohexene hydrogenation in three different solvents as a function of cyclohexene concentration at 70 °C, fitted with Model 3 and Model 4. **(a)** Turnover frequencies (TOF) as a function of H₂ pressure at constant H₂ pressure (38 atm). **(b)** Comparison between turnover frequencies (TOF) obtained from experimental measurements. The fittings were done simultaneously for both sets of data, those of this figure and those of Fig. 1.

Tables 3 and 4 summarize the values of kinetic and adsorption parameters derived from the simultaneous fitting of the data at varying P_{H_2} (constant C_E) and varying C_E (constant P_{H_2}) over the three solvents, using different models (Model 3 and Model 4). The fact that this fitting is done using a single set of parameters must be emphasized as it cross-validates the physical meaning of these parameters. To further assess the quality and reliability of the kinetic and thermodynamic parameters derived from the fit, 95% confidence intervals were calculated for each parameter. They are included in **Tables 3 and 4**, along with the derived parameters.

Table 3. Kinetic Model 3 fitting parameters from isothermal experiments at 70 °C in three different solvents. 95% confidence intervals are indicated for each parameter.

Parameters	Solvent					
	n-heptane HEP		methylcyclohexane MCHA		decalin DL	
	Varying P_{H_2}	Varying C_E	Varying P_{H_2}	Varying C_E	Varying P_{H_2}	Varying C_E
k_3 (s^{-1})	312 ± 27	312 ± 41	312 ± 27	312 ± 122	312 ± 189	312 ± 68
K_{H_2}	0.26 ± 0.6	0.26 ± 1.4	0.26 ± 1.4	0.26 ± 3.0	0.26 ± 4.5	0.26 ± 8.7
K_E	5.6 ± 1.3	5.6 ± 2.9	5.6 ± 1.5	5.6 ± 1.4	5.6 ± 3.7	5.6 ± 1.8
K_S	0.01 ± 0.10	0.01 ± 0.10	0.5 ± 0.02	0.5 ± 0.18	3.7 ± 2.5	3.7 ± 8.7

Table 4. Kinetic Model 4 fitting parameters from isothermal experiments at 70 °C in three different solvents. 95% confidence intervals are calculated for each parameter.

Parameters	Solvent					
	n-heptane HEP		methylcyclohexane MCHA		decalin DL	
	Varying P_{H_2}	Varying C_E	Varying P_{H_2}	Varying C_E	Varying P_{H_2}	Varying C_E
k_4 (s^{-1})	249 ± 102	249 ± 149	249 ± 350	249 ± 95	249 ± 28	249 ± 49
K_{H_2}	0.17 ± 0.003	0.17 ± 0.0003	0.17 ± 0.14	0.17 ± 0.008	0.17 ± 0.025	0.17 ± 0.02
K_E	13 ± 0.1	13 ± 3.5	13 ± 0.03	13 ± 0.24	13 ± 0.04	13 ± 70
K_S	7.5 ± 0.41	7.5 ± 1.5	81 ± 1.4	81 ± 11	581 ± 12	581 ± 16
K_{EH}	48 ± 0.12	48 ± 1.0	48 ± 0.12	48 ± 0.28	48 ± 0.14	48 ± 0.20

It can be seen that Model 3 results in a better fitting than Model 4 when HEP was used as a solvent. This may be due to the weaker interaction between solvent molecules with both reactant

and surface than in the other two solvents. As demonstrated by DFT calculations, on the clean Pd(111) surface (**Figure S5**), the first hydrogenation step has a higher intrinsic reaction barrier than the second hydrogenation. By further increasing the H surface coverage on Pd(111) to 14 H atoms (**Figure S5**) we see that the difference in activation barriers between the two steps is more pronounced. Indeed, the intrinsic activation barrier for the first hydrogenation step drops due to weaker Pd–C and Pd–H bonds that allow a more facile insertion of H into metal–H bond. But the barrier for the second step is reduced to a greater extent. Moreover, as shown in section 3.2 below, all the kinetic and thermodynamic parameters derived from this model are realistic and can be validated by theoretical estimates, which supports the concept that Model 3 is valid in HEP.

While Model 3 satisfactorily describes the reaction in n-heptane (HEP), the situation changes when the solvent adsorbs more strongly on Pd, which is reflected by the strengths of interaction with the surface and quantified by the adsorption constants (K_s) of the solvents derived from the kinetic analysis; that is, $K_{\text{HEP}} < K_{\text{MCHA}} < K_{\text{DL}}$. Particularly for the reactions conducted in DL, Model 4 appears to be significantly better representation than Model 3. The conclusion from this observation is very interesting.

In Model 3, the rate is proportional to θ_{HS1} and θ_{ES2} . The latter contains a solvent adsorption term ($K_s C_s$) that can significantly inhibit the overall rate if it is large enough in comparison to 1 and the other adsorption terms ($K_i a_i$ or $K_i P_i$). By contrast, in Model 4 the second hydrogenation is the rate determining step, with the single hydrogenated intermediate in quasi-equilibrium with ES2 (cyclohexene adsorbed on site 2) and HS1 (hydrogen adsorbed on site 1). In this case, in addition to the adsorption terms for cyclohexene and the solvent, the denominator includes the term $K_{\text{EH}} K_{\text{E}} a_{\text{E}} \sqrt{P_{\text{H}_2} K_{\text{H}_2}}$, which results from the quasi-equilibrium of EHS2 (partially hydrogenated cyclohexene EH on site 2) with ES2 and HS1. That is, despite the assumption that H adsorbs on different sites from the hydrocarbon species and solvent, an increase in H_2 pressure causes a change in the balance of site 2. One could expect that when the reaction is carried out at high enough H_2 pressure, the term $K_{\text{EH}} K_{\text{E}} a_{\text{E}} \sqrt{P_{\text{H}_2} K_{\text{H}_2}}$ should eventually become dominant, making the rate independent of the type of solvent used as $K_{\text{EH}} K_{\text{E}} a_{\text{E}} \sqrt{P_{\text{H}_2} K_{\text{H}_2}} \gg 1 + K_{\text{E}} a_{\text{E}} + K_s a_s$. In other words, the effect of solvent in rate should be less pronounced as the H_2 pressure increases. However, as seen in kinetics fitting, this will only be observable at exceedingly high H_2 pressures.

Moreover, at very low H_2 pressures, Model 4 predicts a first order with respect to H_2 . However, the hydrogen-containing terms in the denominator influence the observed order, even at relatively low pressures; making it difficult to decide which of the two models best represents reality. Interestingly, Gonzo and Boudart, operating at sub-atmospheric P_{H_2} observed a $1/2$ order behavior, which would support Model 3; however, they concluded that the first hydrogenation step could not be rate limiting since they observed that the H/D exchange reaction readily occurs in cyclohexene, indicating that the first hydrogenation is highly reversible. Therefore, they proposed that the RDS was the second hydrogenation despite the observed $1/2$ order. This would only happen if the term $K_{\text{EH}} K_{\text{E}} C_{\text{E}} \sqrt{P_{\text{H}_2} K_{\text{H}_2}}$ in the denominator is much greater than $1 + K_{\text{E}} C_{\text{E}} + K_s C_s$, and at

the same time $\sqrt{P_{H_2}K_{H_2}} \ll 1$. However, using the parameters of our fitting for Model 4 we found no conditions at which this situation could occur. Therefore, for the weaker interacting HEP solvent, Model 3 is a better representation of the real situation, which also agrees with the predictions of the DFT calculations conducted in vacuum, which is a rough approximation of a system with a weakly interacting solvent, such as HEP.

When the solvent (DL) competes strongly for active sites, Model 4 seems to be a better representation of the reaction. As illustrated in **Figure 3** that shows the evolution of coverages as a function of H_2 pressure, the EHS2 (partially hydrogenated cyclohexene EH on site 2) is no longer the most abundant surface intermediate; as a result, the second hydrogenation step, which includes this intermediate as initial state becomes rate-limiting.

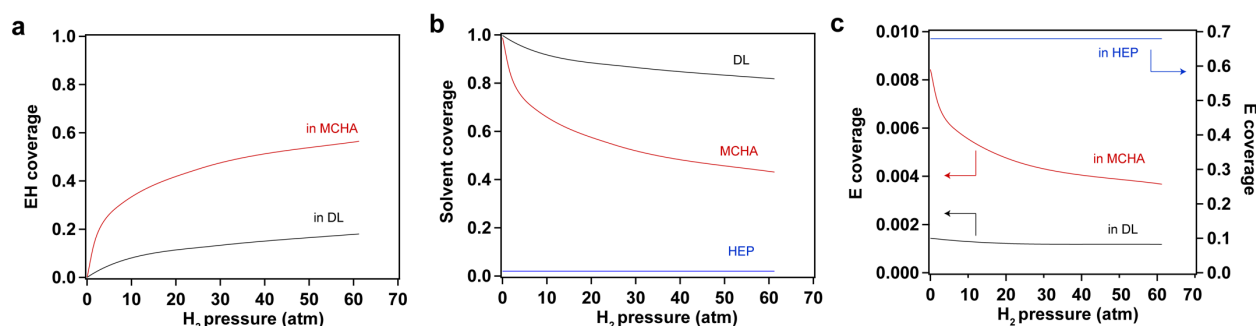


Figure 3. (a) Coverage of partially hydrogenated cyclohexene EH intermediate as a function of H_2 pressure in different solvents; (b) Coverage of solvents as a function of H_2 pressure in different solvents; (c) Coverage of cyclohexene E as a function of H_2 pressure in different solvents. In all cases, coverages in HEP solvent were calculated using Model 3, while those in MCHA and DL solvents were obtained from Model 4.

For MCHA, which shows medium strength of interaction with catalyst surface, both Model 3 and Model 4 can fit the data. This could be due to the competition between solvent molecule and EH on the catalyst surface. As shown in **Figures 3a and 3b**, at low H_2 pressures the EH coverage in MCHA is much less than the solvent coverage, while the opposite is true above 30 atm. As a result, at certain conditions, Model 3 fits better the experimental rate, while at other conditions Model 4 does.

3.2. Thermodynamic parameters derived from kinetics fitting of rate measurements at varying temperatures ($T = 40-100^\circ C$)

A realistic kinetic model not only describes the variation of rates with operational variables (pressure concentration, temperature), but can also be used to determine the thermodynamic parameters associated with the reaction, such as the entropy and enthalpy changes occurring during adsorption and reaction [39]. To obtain these parameters for cyclohexene and hydrogen, we have conducted additional reaction runs in HEP solvent at varying temperatures. Since the adsorption constant of HEP is so small in this model (< 0.01), the rate expression can be simplified as follows:

$$r = k_3 \times \frac{K_E a_E}{1 + K_E a_E} \times \frac{\sqrt{P_{H_2} K_{H_2}}}{1 + \sqrt{P_{H_2} K_{H_2}}} \quad (12)$$

whereas the rate (k_3) and adsorption equilibrium (K_i) constants can be written in terms of the TST and Van Hoff expressions [63]:

$$k_3 = N_s \frac{k_B T}{h} e^{\frac{\Delta S^\ddagger}{R}} e^{-\frac{\Delta H^\ddagger}{RT}} \quad (13)$$

$$K_i = e^{\frac{\Delta S_{ads}}{R}} e^{-\frac{\Delta H_{ads}}{RT}} \quad (14)$$

where N_s , ΔS^\ddagger , ΔH^\ddagger are catalyst site density, entropy and enthalpy of activation. k_B , h , R are Boltzmann constant, Planck constant and gas constant, respectively. The ΔS_{ads} and ΔH_{ads} in the adsorption equilibrium constant represent the entropy and heat (enthalpy) of adsorption. Therefore, the rate expression in equation (12) contains six adjustable parameters; they include the entropies and enthalpies of adsorption for H₂ and cyclohexene, and the entropy and enthalpy of activation for the rate constant of the RDS.

3.2.1. Enthalpy of Adsorption

Our own DFT calculations as well as previous studies involving adsorption of cyclohexene [33, 64], benzene [65, 66], and H [67] indicate that the adsorption enthalpies do not remain constant as the coverage changes. In fact, **Figure S6** shows the different adsorption conformations of cyclohexene on the H-covered Pd(111) surface. While the H atoms do not compete with cyclohexene for the same sites [56], the cyclohexene adsorption strength drops significantly from -137 kJ/mol for the clean surface (**Figure S7**) to -72 kJ/mol at high H surface coverages and to -87 kJ/mol at high cyclohexene coverages. Likewise, **Figure S8** shows that heat adsorption of H drops as a function of H coverage.

We have attempted to fit the data for the different temperatures with variable enthalpies of adsorption. However, the increased number of additional parameters required for this fitting have a very negative impact on the resulting confidence intervals. Therefore, we have made the simplifying assumption of considering constant enthalpies of adsorption, which should be taken as average values over a range of coverages. To minimize the uncertainty in obtaining these parameters, three different sets of operating conditions were employed to find the initial values for the overall regression. In the first set, reaction temperatures were kept low (40–70 °C) while concentration and pressure of reactants were relatively high (0.42 M and 41 atm for cyclohexene and H₂, respectively). Under these conditions, surface coverage of reactants is approaching saturation, so the rate becomes zeroth order and equal to the rate constant of the RDS. In the second set, higher temperatures (70–100 °C) and lower reactant concentrations (0.17 M cyclohexene and 6.8 atm H₂) were employed. In this case, the surface coverages decrease and change significantly with varying conditions, giving us the opportunity to obtain the adsorption parameters from the curve fitting. Finally, in the third set, the temperatures were kept in the high range (70–100 °C),

while only the H_2 was increased (0.17 M cyclohexene and 41 atm H_2) to keep H coverage high but cyclohexene coverage low.

Figure 4 compares experimental turnover frequencies obtained in the three sets of runs at varying temperatures, cyclohexene concentrations, and H_2 pressures in HEP solvent with those predicted by Model 3 (Equation 12), using the adsorption and kinetic parameters summarized in **Section 3.1** (and **Table 5**).

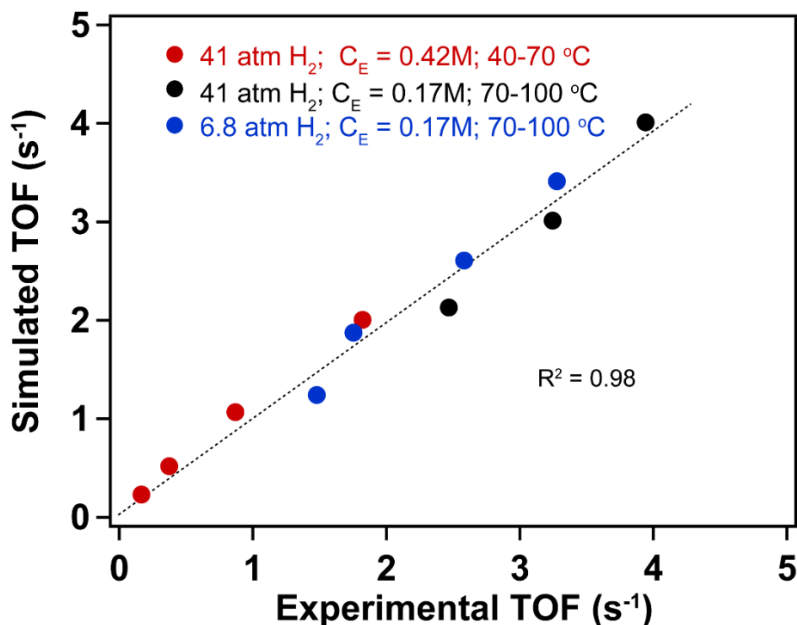


Figure 4. Comparison between turnover frequencies (TOF) obtained from experimental measurements in HEP solvent and those calculated with Equation (12) of Model 3 using parameters summarized in **section 3.2**. Red symbols: Runs conducted in the high pressure of H_2 / high concentration of cyclohexene (C_E)/low temperature region to derive initial values for rate constants; Black and blue symbols: Runs conducted in the low and high pressure of H_2 /low concentration of cyclohexene (C_E)/high temperature region to derived initial values for adsorption equilibrium constants.

One must note that the expression used to fit experimental rates includes the individual kinetic constant, containing the true enthalpy of activation of the rate determining step derived from TST, rather than apparent activation energy usually determined from pseudo-first order kinetic analysis. Therefore, the enthalpy of activation obtained experimentally can be directly compared to energy barriers calculated by DFT. Similarly, the adsorption constants obtained from this expression can be directly compared to the DFT calculations. A detailed discussion of this comparison is offered in section 3.2.3.

Table 5. Kinetic and thermodynamic parameters from experimental fittings at varying temperature (40-100°C) in liquid phase (n-heptane solvent). 95% confidence intervals are indicated for each parameter.

Parameters	Adsorption of Reactants from liquid phase (HEP solvent)		Kinetic barriers
	Hydrogen	Cyclohexene	
Enthalpy ΔH (kJ/mol)	- 31 ± 17	-51 ± 0.1	70 ± 5.6
Entropy ΔS (J/mol/K)	- 80 ± 49	- 135 ± 0.5	-30 ± 15

3.2.2. Entropy of adsorption

The entropy changes obtained from the kinetics fitting for adsorption of cyclohexene (-135 J/mol/K) and hydrogen (-80 J/mol/K) can be compared to the absolute entropy values for liquid cyclohexene (237 J/mol/K) and gaseous hydrogen (135 J/mol/K) at 70°C [68, 69], to which each reactant and their adsorption constants are referenced to, respectively. These results indicate that the adsorbates lose about 2/3 of their initial entropy; that is, both cyclohexene and hydrogen 60 %.

To determine whether these estimates for entropy losses upon adsorption are realistic we have conducted some statistical mechanics analysis. The adsorption equilibrium constant can be expressed in terms of partition functions of adsorbed species and free molecules as follows [39, 63, 70, 71]:

$$K_i = \frac{Q_{ads}}{Q_{gas/liquid}} e^{-\frac{\Delta H_{ads}}{RT}} = A_{ads} e^{-\frac{\Delta H_{ads}}{RT}} \quad (17)$$

$$Q = q_t q_r q_v \quad (18)$$

$$A_{ads} = \frac{q_{t,ads} q_{r,ads} q_{v,ads}}{q_{t,gas/liquid} q_{r,gas/liquid} q_{v,gas/liquid}} \quad (19)$$

Where q_t, q_r, q_v are respectively the translational, rotational and vibrational partition functions, and Q_{ads} and $Q_{gas/liquid}$ are the canonical partition function of the adsorbed molecule and the free molecule in the gas or liquid, respectively.

The following equations were used to calculate partition function for each mode of the polyatomic molecules:

$$q_t^{1DOF} = l \frac{(2\pi m k_B T)^{1/2}}{h} \quad (20)$$

$$q_r^{3DOF} = \frac{1}{\sigma} \left(\frac{8\pi^2 k_B T}{h^2} \right)^{3/2} \sqrt{\pi I_A I_B I_C} \quad (21)$$

$$q_v = \frac{1}{1 - e^{-h\nu/k_B T}} \quad (22)$$

where l is the range of one-dimensional motion of a particle of mass m , I_A, I_B, I_C are moments of inertia for a larger molecule along the three principal axes; σ is a symmetry factor and ν is the vibrational frequency of each vibrational mode. To obtain q_t of cyclohexene in the liquid phase, a molecule is considered to move with 3 degrees of freedom (DOF) inside a volume V , which can be calculated according to

$$V = \frac{MW}{\rho} \frac{1}{N_A} \quad (23)$$

where ρ and MW are the cyclohexene density and its molecular weight, N_A is the Avogadro constant. This gives an estimated V of 0.168 nm^3 . The symmetry factor σ for cyclohexene in rotational partition function Eq. (21) is 2 [72]. I_A, I_B are moments of inertia around the axes on the same plane as cyclohexene, while for I_C it is perpendicular to the plane. The resulting values are $106.6 \text{ u}\text{\AA}^2$, $111.2 \text{ u}\text{\AA}^2$, $197.2 \text{ u}\text{\AA}^2$ [73]. The vibrational partition function Eq. (22) can be approximated as 1 since the wavenumbers of cyclohexene are relatively high, so $e^{-h\nu/k_B T} \ll 1$.

Using DFT calculations, we compared six different configurations for the adsorption modes of cyclohexene on Pd(111), four of them di- σ (bridge) and two π (atop). **Figure S6** show that the π -B mode is the most stable configuration, with an adsorption energy of -137 kJ/mol . It is usually assumed that [33, 64], upon adsorption, cyclohexene can move around the surface within an area A , which can be estimated by a square of dimensions $l \times l$. It is reasonable to assume that the translational length that adsorbed cyclohexene can diffuse from a top site to its adjacent top site on a Pd (111) surface is the diameter of the Pd atom, which rounds up to about 3 \AA . When the surface coverage of cyclohexene increases, the attractive-repulsive interaction hinders the mobility of cyclohexene and therefore the translational length may decrease. As for the rotational partition function of adsorbed cyclohexene, the π bonding adsorption geometry leads to 2 DOF or less. However, one of the axes has shifted from the center of the cyclohexene molecule in the liquid phase to the C=C bond on the surface. The moments of inertia produced under the adsorbed state needs to be recalculated using the point mass of cyclohexene and the distance to C=C bond axis [74]. The rotational DOF are also influenced by the surface coverage and eventually adsorbed cyclohexene reduces to zero DOF. The vibrational partition function $q_{v,ads}$ can be written as $q_{v,gas/liquid} q_{v,C-Pd}$. Due to the formation of C-Pd bonds, cyclohexene gains additional vibrational modes upon adsorption on Pd. Previous studies of ethylene adsorption on Pd (111) [75] have shown that the vibrational frequencies for C-Pd are 341 cm^{-1} and 533 cm^{-1} . Thus, for the vibrational partition function $q_{v,C-Pd}$ we have used 400 cm^{-1} for both C. Combining Eqs. (20) - (23), Eq. (18) for cyclohexene adsorption becomes:

$$A_{ads}(T = 343K) = \frac{q_{t,ads}^{2DOF} q_{r,ads}^{2DOF} q_{v,gas/liquid} q_{v,C-Pd}}{q_{t,liquid}^{3DOF} q_{r,liquid}^{3DOF} q_{v,liquid}}$$

$$= \frac{(l \times 9.61 \times 10^{10})^2 \times (37.80 \times 39.66) \times (1.23 \times 2)}{1.68 \times 10^{-28} (m^3) \times (9.61 \times 10^{10})^3 (m^{-3}) \times (34.42 \times 39.66 \times 52.81)}$$

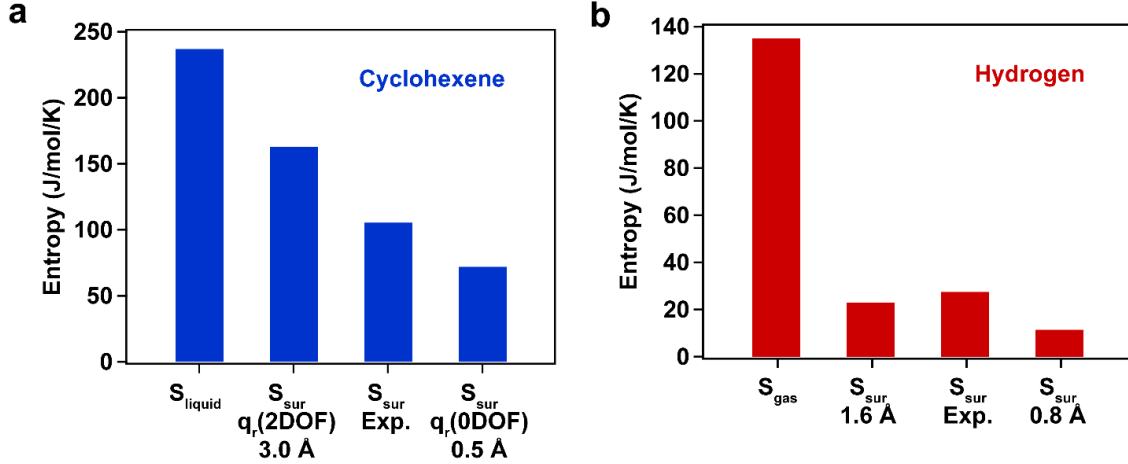


Figure 5. (a) Calculated entropies of adsorbed cyclohexene for two different translational lengths and rotational DOF compared to that derived from experimental data and the entropy of cyclohexene in the liquid phase (S_{liquid}). (b) Calculated entropies of adsorbed hydrogen for two different translational lengths compared to that derived from experimental data and the entropy of hydrogen in the gas phase (S_{gas}).

Equation (17) shows that A_{ads} is the entropic pre-exponential factor for the equilibrium constant. From the analysis above, we see that the major contributions to the adsorption entropy change arise from changes in the translational length and the number of rotational DOF left in the molecule upon adsorption. Therefore, depending on what assumptions one makes regarding these two parameters (l and DOF), the entropy of the adsorbed species can change significantly. The resulting entropies for adsorbed cyclohexene and hydrogen are compared in **Figure 5**, along with the entropies of liquid cyclohexene and gaseous hydrogen, respectively. Clear trends are observed. For example, for cyclohexene, longer translational lengths and higher DOF for rotations represent higher mobility retained by the adsorbed cyclohexene. Therefore, as depicted in **Figure 5a**, when the adsorbed cyclohexene has the ability to diffuse from one top site to another with a length of 3 \AA as well as rotating around two axes, it retains an entropy of 163 J/mol/K , corresponding to an entropy loss of -74 J/mol/K (or 30 % of the original entropy). At the other extreme, when the adsorbed cyclohexene molecule is more restricted to move or rotate freely, ($l = 0.5 \text{ \AA}$ and zero rotation DOF), the amount of entropy retained by the surface species is 73 J/mol/K , which corresponds to an adsorption entropy change of -164 J/mol K (or 70 % of the original entropy in the liquid phase, 237 J/mol K). As shown in **Figure 5a**, the experimentally derived entropy of the adsorbed cyclohexene (102 J/mol/K) is in good agreement with the latter assumption of a more

restricted adsorbate. Campbell and Sellers [76] quantified the entropies of adsorbed alkanes on Pt (111). They demonstrated that, in that case, the adsorption entropy drops were only around 1/3 of the original gas entropy and concluded that this loss was mostly associated with the freeze of motion in the z direction. In our case, the observed entropy loss is relatively larger compared to the original entropy in the liquid phase. A much stronger bonding of alkenes on Pd compared to Pt may lead to restrictions not only on the z direction, but also on the x and y directions.

Similarly, the pre-exponential factor for gas phase H_2 adsorption obtained experimentally (**Table 5**) can be compared with the values derived using partition functions. Adsorbed hydrogen atoms only possess translational degrees of freedom and vibrations of newly formed H-Pd surface bonds, with no contributions from rotation. To estimate the translational DOF, we analyzed the H diffusion barriers on Pd (111) calculated by DFT. The preferential site for H adsorption on Pd (111) is the fcc hollow site. The lowest energy pathway for the diffusion of adsorbed H is passing through the bridge site to an hcp site [56, 77]. The energy barrier for this path is 12 kJ/mol. By contrast, the path that goes through an atop site is about 47 kJ/mol [56]. The distance between an fcc site to a bridge site is 0.8 Å and to a hcp site is 1.6 Å. Therefore, the translational length l for adsorbed H may not be more than 1.6 Å. Gas phase H_2 molecule moves in a volume of V , which can be approximated using ideal gas law at the standard pressure. The rotational partition function is only considered for the gas phase diatomic H_2 , which has 2 DOF along the axes and a resulting q_r of 2.61 at 343 K [70], while there is no rotational contribution for the two adsorbed H atoms. This difference causes a significant loss in entropy upon adsorption. By contrast, there is no losses in vibrational modes as the vibrational partition functions for both gas phase H_2 and the two adsorbed H are assumed to be the same. Therefore, the pre-exponential factor for $H_2 + 2S \rightleftharpoons 2HS$ becomes:

$$A_{ads}(T = 343K) = \frac{Q_{ads}}{Q_{gas}} = \frac{(q_{t,ads}^{2DOF} q_{v,ads})^2}{q_{t,gas}^{3DOF} q_{r,gas}^{2DOF} q_{v,gas}}$$

$$= \frac{[(l \times 1.50 \times 10^{10})^2]^2}{\frac{k_B T}{p^0} (m^3) \times (1.50 \times 10^{10})^3 (m^{-3}) \times 2.61}$$

Solving for the entropy of adsorption using Eq. (14), the results are plotted in **Figure 4b**. Depending on the assumption for the value of l , we obtain a residual entropy for the adsorbed H of 21 J/mol/K (when $l = 1.6$ Å) or 9.5 J/mol/K (when $l = 0.8$ Å). The former would represent an H atom moving from an fcc site to an hcp site through a bridge site, while the latter would be when it moves from fcc to a bridge site. The corresponding values for the entropy losses in these two cases upon adsorption are -93 J/mol/K (relative to the gaseous H_2) in the first case and -116 J/mol/K in the second. Therefore, the value derived from the experimental kinetic fitting (see **Table 5**) -80 J/mol/K (relative to the gaseous H_2), which gives a residual surface entropy of 27.5 J/mol/K is consistent with the prediction of a rather mobile adsorbed H, moving between an fcc and an hcp sites ($l = 1.6$ Å). These results are in the same range as the value reported for the adsorption of H over Pd black (entropy of adsorption = -90 J/mol/K) [78].

3.2.3. Entropy-Enthalpy Correlation

To further evaluate the physical consistency of the thermodynamic parameters derived from the kinetics, we have compared them with a set of guidelines used by Boudart [1, 2] to compare the entropy of adsorption with the heat of adsorption. That is, entropy of adsorption follows an empirical correlation with heat of adsorption: $-\Delta S = 51 - 0.0014 \Delta H$ (in J/mol K) [71]. As shown in the **Figure 6**, the pairs of entropy/enthalpy of adsorption derived from our kinetic analysis correlate very well with this correlation, giving validation to the physical meaning of the kinetics fitting.

We can also use this correlation [4, 71, 79] to further compared the validity of Models 3 and 4 for each solvent since we have the adsorption parameters for the solvents derived from the kinetics fitting with each model and can compare them to those of the reactants, obtained experimentally by varying temperature.

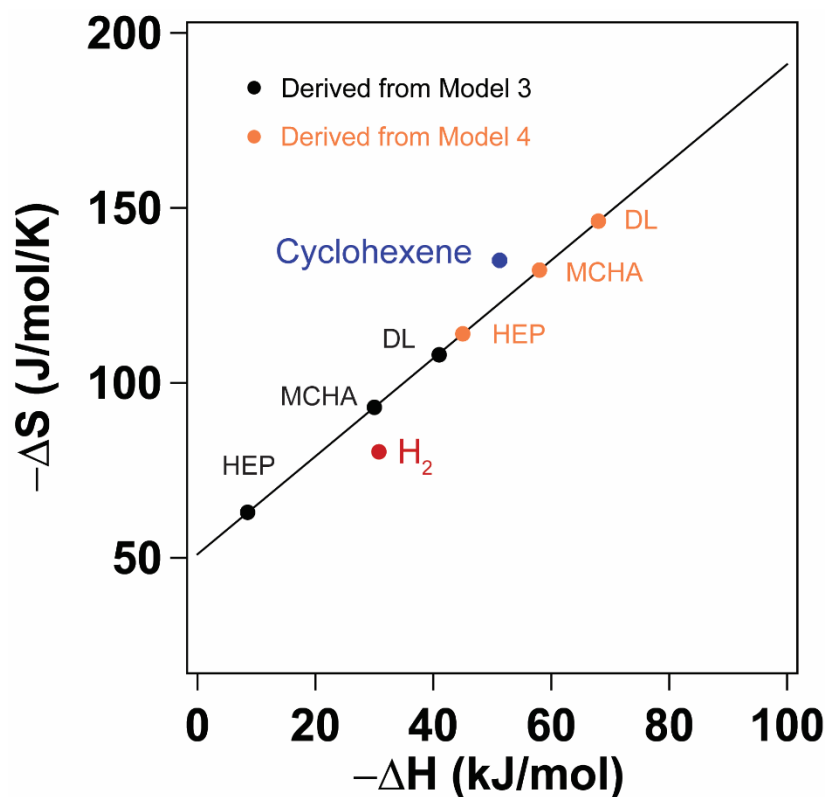


Figure 6. Comparison between the experimental adsorption enthalpy and entropy obtained for reactants H₂ (red circle) and cyclohexene (blue circle) and the correlation proposed by Boudart [4, 71, 79] ($-\Delta S = 51 - 0.0014 \Delta H$ (in J/mol K)). The ΔS and ΔH values for the three solvents were obtained by using this correlation and the experimental adsorption constants (K_i) derived from kinetic analysis for each solvent with Models 3 and 4.

Interestingly, the n-heptane (HEP) adsorption constant derived from Model 3 is $K_{\text{HEP}} = 0.01$ and using the Boudart's entropy/enthalpy correlation, the resulting entropy and enthalpy of adsorption would be -63 J/mol K and -8.5 kJ/mol, which is consistent with a very weak interaction of the HEP solvent with the surface. By a similar analysis, we obtain adsorption entropies of -93

and -108 J/mol K and adsorption enthalpies of -30.2 and -40.8 kJ/mol, for MCHA and DL, respectively. Likewise, the numbers for enthalpy and entropy of adsorption derived from Model 4 for HEP, MCHA, and DL are -45 kJ/mol and -113 J/mol/K, -58 kJ/mol and -131 J/mol/K, and -68 kJ/mol and -147 J/mol/K, respectively.

Adsorption enthalpy values reported in the literature from experimental/theoretical adsorption measurements on clean Pd(111) crystals are qualitatively consistent with this trend; that is linear alkanes < cyclohexanes < double rings. For example, microcalorimetry measurements yielded a heat of adsorption of ~ 80 kJ/mol for the adsorption of n-hexane on a Pd/SiO₂ catalyst [80], while DFT calculations predict a heat of adsorption of ~ 134 kJ/mol for 1,2-dimethylcyclohexane on Pd(111) [81] and 191 kJ/mol for decalin [82], both on Pd(111). However, these values are significantly higher than those derived in this study from reaction kinetics in the liquid phase. This discrepancy has several potential causes that need to be considered: (1) solvation effects. An adsorbed molecule at the liquid-solid interface exhibits a lower extent of solvation than the molecule in the bulk of the liquid, to which is referred to in the kinetic analysis. Therefore, as proposed by Campbell et al. [32, 33] even considering the same strength of interaction between the adsorbate and the surface, the differential solvation causes a great decrease in the observed heat of adsorption. (2) co-adsorption of hydrogen. As demonstrated by the DFT calculations shown in the Supplementary Information and discussed above, the presence of hydrogen on the surface causes a strong decrease in heat of adsorption of all hydrocarbons. (3) coverage effects of all hydrocarbon species (cyclohexene and solvent molecules). Again, DFT calculations show that at higher coverages, the heats of adsorption of a given molecule greatly decreases. (4) At the high H₂ pressures and relatively low temperatures of the experiments, Pd may be partially or fully converted into Pd hydride [83]. As shown in **Figure S5** in Supplemental Material, a significant drop in heat of adsorption is observed when the Pd(111) surface is replaced by a PdH surface. With all these considerations we can safely conclude that the enthalpies and entropies of adsorption derived from the kinetic analysis are physically realistic.

Moreover, the trends in enthalpy of adsorption of the different solvents observed in **Figure 6** can be used to give further support to the conclusions derived from the kinetic fitting on which kinetic model was more appropriate. For instance, Model 3 was found to better fit the kinetic data when HEP was the solvent. The much lower heat of adsorption for HEP than for cyclohexene is consistent with the expectations based on the above discussion. On the other hand, Model 4 was found to result in a much better fit of the kinetic data when DL was the solvent. Again, in **Figure 6**, the resulting heat of adsorption, higher than that of cyclohexene is consistent with the drastic rate losses observed with this solvent. By contrast, Model 3 for DL would predict a heat of adsorption lower than that of cyclohexene, which would not be consistent with a strong competitive adsorption.

3.2.4 Entropy and enthalpy of activation

As listed on **Table 5**, the kinetic entropy and enthalpy of activation derived from the experimental rate constants obtained at varying temperatures were -30 J/mol/K and 70 kJ/mol,

respectively. Since Model 3 indicates that the first hydrogenation is rate-determining, the initial state for this step contains a cyclohexene molecule and a hydrogen atom on contiguous (different) sites. The resulting small and negative entropy of activation indicates that the entropy of the transition state decreases slightly relative to the separate adsorbed species. This is the result of two contributions; one is a decrease in entropy as two independent species become essentially one, the other is an increase in entropy as the activated complex C_6H_{11} gains additional degrees of freedom as the ring becomes more saturated with hydrogen [84]. Overall, the small and negative entropy of activation from the experimental fitting indicates that these two effects balance out, with the weakening of the surface interaction at the transition state being slightly less important than the loss of entropy.

DFT calculations in **Figure S5** shows that on 14H covered PdH surface, intrinsic activation barrier was 80 kJ/mol for the first hydrogenation step and 60 kJ/mol for the second hydrogenation step, with the first one being RDS. This result is in good agreement with the experimental value obtained from kinetics fitting (70 kJ/mol). This result gives more support to the idea that under our reaction conditions, Pd is in the form of hydride. But the difference between these two steps is small. Therefore, when the surface coverage of EH intermediate drops caused by competitive adsorption with the more strongly adsorbed solvent molecules (MCHA and DL), the reaction kinetics can easily shift from first hydrogenation to second hydrogenation step, as suggested by the better quality of the fit for these two cases.

3.3. Non-ideality in solvent effects on cyclohexene hydrogenation rate in liquid phase

Another complication that arises when changing solvents is the possibility of forming a non-ideal mixture. In that case, to consider thermodynamic non-idealities the adsorption equilibrium constants should be expressed in terms of thermodynamic activities, which take into account the solvent-solute and solvent-solvent interactions that may affect the surface coverage of species, and consequently, the rates [61]. To further demonstrate the effect of solvent competitive adsorption, cyclohexene hydrogenation was conducted in several mixtures of solvents. In this series of experiments, HEP was chosen as the primary solvent since its adsorption competition is negligible compared to the cyclohexene reactant. A secondary solvent was added to create a solvent mixture with varying compositions from pure HEP to the pure secondary solvent. Both ideal and non-ideal conditions are considered to fit the experimental data. The activity coefficients of HEP and secondary solvents are equal to 1 for the ideal conditions fitting, while the activity coefficients were obtained from the UNIQUAC model in ASPEN Plus for the non-ideal conditions fitting. By using the kinetic parameters (shown in **Table 3**) and rate expression of Model 3 (equation 12), the hydrogenation rates in co-solvent mixtures under both ideal and non-ideal conditions are predicted.

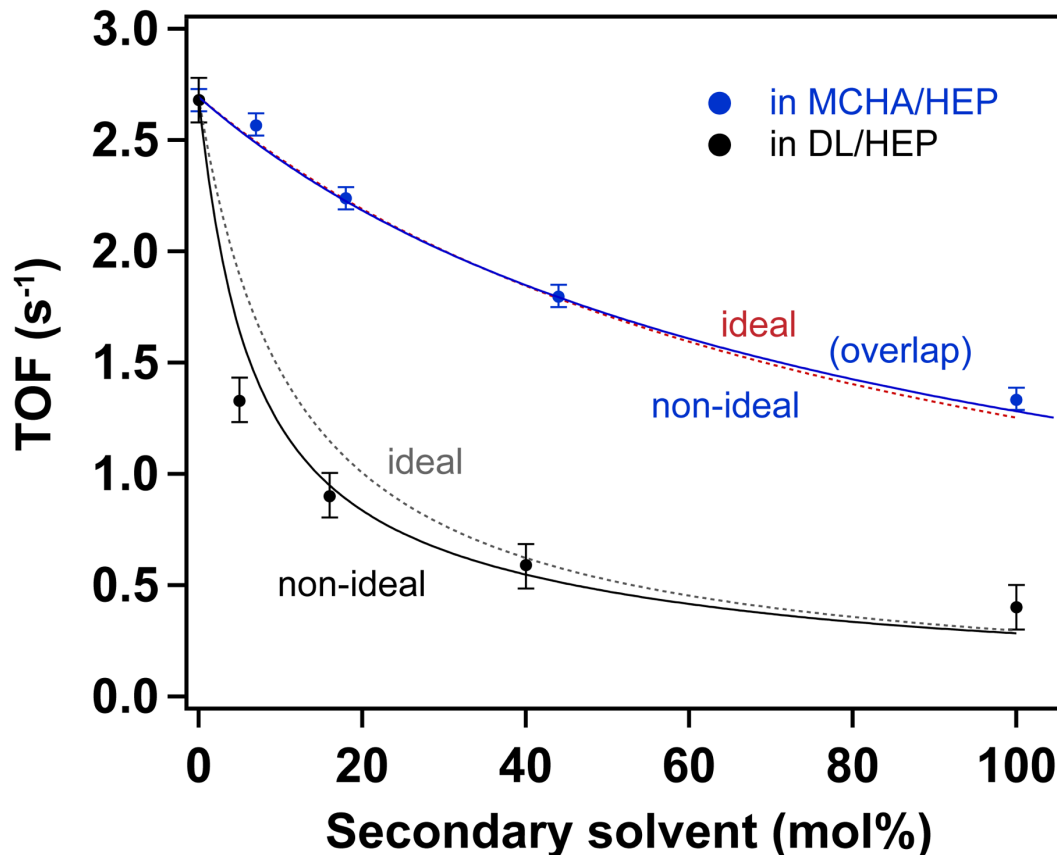


Figure 7. Hydrogenation of cyclohexene in co-solvent mixtures (MCHA/HEP and DL/HEP). Dashed lines are fitting curves by considering the co-solvents as ideal mixtures (the activity coefficients of all the solvents are 1); solid lines are fitting curves by considering the co-solvents as non-ideal mixtures (with varying activity coefficients obtained from ASPEN Plus UNIQUAC model). Reaction conditions: temperature 70 °C, H₂ pressure 38 atm. (Error bars were determined by standard derivation).

The results are shown in **Figure 7** for the MCHA/HEP and DL/HEP mixtures. The rate drops gradually in both cases as the fraction of the secondary solvent, which adsorbs more strongly than the primary solvent, increases; however, the goodness of the fitting varies significantly from one to the other. That is, when using the rate expression for Model 3 shown in **Table 2**, the fitting for the MCHA/HEP solvent system is excellent, even when considering an ideal mixture where $a_{solvent} = C_{solvent}$. However, this is not the case for the DL/HEP solvent system, for which the fitting is significantly poorer when considering an ideal mixture, but excellent when a non-ideal system is used.

Clearly, the DL/HEP solvent mixture is highly non-ideal with positive deviations from Raoult's law [85]. As the concentration of the secondary solvent increases in the binary mixture from 0 to 1, the activity coefficient changes from its value at infinite dilutions to 1, as the mixture approaches the pure secondary solvent. For example, values derived from ASPEN Plus indicate the $\gamma_{decalin}$ starts at 1.52 at decalin concentration ~ 0 but drops to ~ 1.16 when decalin

concentration is 40 mol % and to 1 when it approaches 100 % (see **Figure S9** in Supplementary Material).

Since the liquid bulk phase is in equilibrium with the catalyst surface, the total number of surface species is affected by changes in the thermodynamic activity of the solvents. When DL is added in HEP, the solvent interactions increase the repulsion of DL away from the liquid bulk phase onto the catalyst surface, leading to an increased surface concentration of DL. Therefore, the kinetic model of ideal mixture (dash line in **Figure 7**) that applies concentration instead of activity does not describe the experimental data well enough because the catalyst surface has more DL to compete sites with cyclohexene than in ideal mixture. The deviation from the ideal case is more pronounced in the 0–40 mol.% DL range, where the actual hydrogenation rate is much lower than that predicted from the ideal solution model. In this range, above 40 mol.% DL, the rate in ideal mixture. On the other hand, the MCHA/HEP mixture activity coefficients are close to unity with $\gamma_{MCHA} = 1.04$ and $\gamma_{HEP} = 1.02$ at infinite dilution, so, the mixture does not deviate from the ideal solution. Therefore, using kinetics in terms of concentrations captures the experimental data very well.

Table 6. Surface coverage in different solvents derived from Model 3. ^a

Adsorbates	Coverage in single solvent			Varying Co-solvent mixture ^b	
	n-heptane HEP (%)	methylcyclohexane MCHA (%)	decalin DL (%)	95 % HEP 5 % DL	95 % HEP 5 % MCHA
H ₂ (site 1)	76	76	76	76	76
Vacant (site 1)	24	24	24	24	24
Cyclohexene (site 2)	71	33	12	43	67
Primary solvent (site 2)	0	52	85	0	0
Secondary solvent (site 2)	-	-	-	39	5
Vacant (site 2)	29	14	3	18	28

^a Reaction conditions: 70 °C, 38 atm H₂, C_E = 0.42 M.

In the DL/HEP system, the presence of decalin alters the catalyst surface coverage since it strongly competes with the other surface species. **Table 6** compares the surface coverages under the same reaction conditions (38 atm H₂ and 0.42 M cyclohexene) for the different solvent systems, calculated using the adsorption parameters in **Table 3**. In pure solvents, the cyclohexene surface coverage significantly drops as the solvent is changed from HEP (71%) since the solvent does not adsorb. When 5 mol.% DL was introduced, cyclohexene coverage is reduced to 43%, which explains the drastic decrease in hydrogenation activity. In contrast, when a 5 mol% MCHA in HEP solvent mixture is used, the much weaker adsorption of MCHA causes only a minor drop in cyclohexene, which now only drops to 67%, consistent with a more modest decrease in hydrogenation activity.

In summary, since the activity coefficients of both cyclohexene and any of the non-polar solvents are all close to 1, the effects of non-idealities are not significant for pure solvents. That is, the influence of solvent-reactant interactions is negligible on the hydrogenation rate. However, for reactions involving two solvents mixture, the non-ideality of the solvent mixture can have drastic effects on activity.

3.4. Effect of polarity and non-idealities on liquid phase hydrogenation of C=C and C=O bonds

We have shown above that in systems of non-polar reactants and non-polar solvents, the major effect of the solvent is competitive adsorption; also, when non-idealities are present, the major effect is the modification of the effective surface coverages of reactants and solvents relative to the ideal case. However, when polar reactants or polar solvents are involved, other phenomena can become important. For example, in a recent study, we combined reaction kinetics and computational calculations to show that the presence of water provides an additional reaction pathway with a lower activation barrier for the hydrogenation of furfural catalyzed by Pd [86]. In the reaction pathway derived from that study, an adsorbed H atom is picked up as a proton by the solution and, upon charge separation, it is transferred to the C=O group of furfural through the liquid phase, assisted by a H-bonded water network. By contrast, hydrogenation of the C=C bond is not influenced by the presence of water due to the lack of a polar group and the absence of H-bonded channels in this part of the reaction pathway. More often than in metal-catalyzed reactions, proton transfer phenomena have been reported for reactions catalyzed by Brønsted acid sites, such as dehydration [87] and aldol condensation [29, 31]. For example, we have recently reported that a small amount of water enhances the self-condensation of cyclopentanone (CPO) on MCM-41-SO₃H catalysts with low acid density in which the sites are not adjacent [31]. In this case, water helps bridging active sites that are not forming pairs on the surface and extending the polarizing effect to the carbonyl group of the CPO; this facilitates the rate limiting C–C coupling step. As a result, the cooperative catalysis action between two sites becomes possible, and the reaction kinetics in the presence of water switches from a bimolecular single-site mechanism to a bimolecular dual-site mechanism.

Here, we have compared the hydrogenation of benzene and benzaldehyde, two molecules with similar aromatic structures but with very different polarity. We have compared the effects of changing the non-polar solvent, using the same three solvents as those used with cyclohexene which exhibit varying strength of interaction with the Pd surface (HEP < MCHA < DL). We have also added water in the mixture to explore how the presence of a polar-protic compound changes the relative reactivity. The two reactions gave just a single product in each case; that is, benzene hydrogenation only yields cyclohexane and benzaldehyde only yields benzyl alcohol. The latter may be due to the preferential orientation of the benzaldehyde molecule at high coverages with the C=O bond pointing down and the aromatic ring away from the surface.

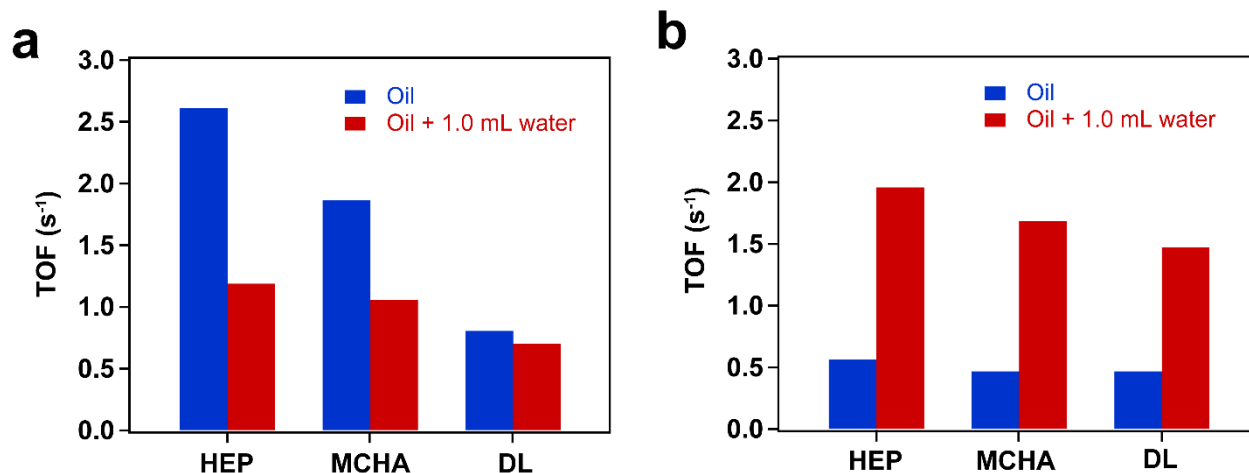


Figure 8. Pd-catalyzed hydrogenation of benzene (a) and benzaldehyde (a) in three different solvents with (red bars) and without (blue bars) addition of 1 mL water. Reaction conditions: 50 mg 1.0 wt% Pd/ α -Al₂O₃ catalyst, 70 °C, 41 atm H₂, 30 min. Volume of solvent: 100 mL

Table 1 shows that benzene, as a non-polar reactant, has activity coefficients close to 1 at infinite dilution in all three non-polar solvents and forms ideal mixtures with them. Therefore, the benzene hydrogenation reaction in the three non-polar solvents follows the same trend in reactivity as that of cyclohexene hydrogenation; that is, n-heptane > methylcyclohexane > decalin, as shown in **Figure 8a** (blue bars). By contrast, benzaldehyde, as a polar reactant with much higher activity coefficients in all three solvents, shows a greater deviation from the ideal behavior compared to benzene. As a result, all these solvents repel the benzaldehyde from the bulk of the liquid onto the Pd surface more effectively; thus, for a given liquid-phase reactant/solvent concentration ratio a higher surface coverage of benzaldehyde than the solvent molecule is obtained, lessening the effect of the strong competitive adsorption of solvents like MCHA and DL. In consequence, this non-ideality makes the solvent effects on benzaldehyde hydrogenation to be less significant, resulting in more similar conversions for all three solvents than for the ideal case, as shown in **Figure 8b** (blue bars), compared to **Figure 8a** (blue bars).

Remarkably, when a small amount of water was added into the non-polar solvent, the benzaldehyde hydrogenation was greatly enhanced (See red bars in **Figure 8b**). This promotion can be explained by the water-mediated proton transfer mechanism and charge separation that we and others have recently demonstrated in the hydrogenation of carbonyls in the presence of water [86, 88, 89]. As mentioned above, the presence of water provides a more effective path for the hydrogenation of carbonyls. Specifically, an adsorbed H atom is transferred as a proton to a water molecule in the liquid phase; there, it is transported to the O of the carbonyl via a H-bonded chain of water molecules, while the separated electron is transferred through the metal. The calculated energy barrier for this concerted path is much lower than the direct hydrogenation by a surface H [86], which explains the observed activity promotion.

By contrast, hydrogenation of the aromatic C=C bonds is not enhanced by the presence of water since this part of the molecule does not form H-bonds with water. Therefore, the activity of ring hydrogenation decreases in the presence of water, which only acts inhibiting active sites on

the surface, as shown in **Figure 8a** (red bars). Moreover, the non-ideality of water/organic mixtures enhances the repulsion of water molecules in the bulk of the liquid pushing them onto the Pd surface, further enhancing the competition for adsorption sites with the reactant. The relative extent of water inhibition varies with the strength of the non-polar solvent-catalyst interactions. That is, water causes a drastic decrease in activity in the case of n-heptane, which by itself does not compete for sites. By contrast, the relative decline in rate (red bars Vs blue bars in **Figure 8a**) is less pronounced with methylcyclohexane, and particularly with decalin, because they already compete strongly for sites with the reactant.

4. Conclusion

In this contribution, we have combined experimental kinetic analysis and DFT calculations to investigate solvent effects on C=C and C=O bond hydrogenation, using cyclohexene, benzene and benzaldehyde as probe reactants in different solvents. Cyclohexene and benzene form ideal mixtures with all non-polar solvents; thus, the C=C bond hydrogenation in a solvent follows the trend HEP>MCHA>DL, which is the trend of increasing solvent interaction with the metal surface.

Analysis of the reaction kinetics indicates that H adsorption occurs on different sites from cyclohexene and solvent and the rate determining step is the first hydrogenation of the C=C bond when the solvent is the non-interacting HEP. By contrast, with more interacting solvents (MCHA and DL), the rate limiting step shifts to the second hydrogenation. The observed solvent effect on observed activity is explained by competitive adsorption of the solvent, which alters the surface coverage of the cyclohexene reactant and the partially hydrogenated reaction intermediate.

The heats of adsorption are coverage-dependent. Hydrogen and cyclohexene adsorb more strongly at low coverages (heats of adsorption of 31 and 137 kJ/mol, respectively); but, as coverage approaches saturation, the heat of adsorption decreases to 24.3 kJ/mol for hydrogen and 64 kJ/mol for cyclohexene, a result validated by DFT calculations. At the same time, the activation barrier reaction diminishes as more H is co-adsorbed on the surface. Comparing the thermodynamic parameters derived from the kinetic fitting with partitions functions we conclude that the adsorbed cyclohexene molecule can have a very low translational mobility, around 0.5 Å in length. The adsorbed H is less restricted, with a translational mobility around 1.6 Å.

Non-idealities may play an important role in mixtures of solvents. Reactions in only one solvent result in negligible deviation from ideal solution since activity coefficients are close to unity. However, the co-solvent DL-HEP mixture is highly non-ideal. The interactions between decalin and n-heptane tend to preferentially drive decalin onto the catalyst surface and compete more effectively for sites with cyclohexene, which leads to further decrease in activity.

By contrast, the non-ideality of the benzaldehyde/solvent mixtures causes an enhanced benzaldehyde coverage reducing the competitive adsorption of the solvent, which yields similar activities in all solvents. Likewise, the non-ideality of water-organic co-solvent leads to the competitive adsorption of water; this explains the decreased activity for benzene hydrogenation in the presence of water. Contrarily, the conversion of benzaldehyde increases in the presence of water. In this case, the H-bonded network at the liquid/solid interface provides an additional

reaction path, facilitating the H transfer to the hydrophilic O atom in the C=O bond with a lower activation barrier, promoting the C=O hydrogenation.

Therefore, the non-ideality of a solution could play an important role in liquid phase reactions. By tuning the composition of the solvents, one could tailor the non-ideality effects of reactant-solvent mixtures to influence the coverage of surface species and consequently the reaction kinetics and catalytic performance.

Acknowledgements

This work was supported by the U.S. Department of Energy, Office of Science, Basic Energy Sciences under Award Number DE-SC0018284. The computational research used supercomputer resource of OU Supercomputing Center for Education & Research (OSCER) at the University of Oklahoma and the National Energy Research Scientific Computing Center (NERSC).

Personal Acknowledgement by Professor Resasco

While I was not a direct disciple of Prof. Michel Boudart, I was greatly influenced by his teachings, his remarkable talks, and especially his books and papers. I have always tried to follow and pass on to my students his recommendations to analyze the catalytic phenomena following thorough thermodynamic and kinetic formalisms. His insistence on the necessity of describing observed catalytic rates in terms of the turnover frequencies of kinetically relevant elementary steps paved the way for modern DFT and microkinetic studies of heterogeneous catalysis; for which we all owe him a debt of gratitude.

In 1983, after finishing my PhD and just as I was starting my academic career in Argentina, my wife and I had the pleasure of acting as informal guides to Michel and Marina during a conference in San Luis. We had an enjoyable and stimulating trip through the mountains with them. Knowing that I was starting my career as an independent researcher, at one point Michel offered me some wise words to help me with choosing my first research project. He said: “it should be a project that is relevant to your country and your region, but at the same time, with enough fundamental content to serve as a tool, first for you to learn, then to teach.” His insightful advice that day is something that I have always treasured.

References

- [1] R. Madon, J. O'connell, M. Boudart, Catalytic hydrogenation of cyclohexene: Part II. Liquid phase reaction on supported platinum in a gradientless slurry reactor, *AIChE Journal*, 24 (1978) 904-911.
- [2] E. Gonzo, M. Boudart, Catalytic hydrogenation of cyclohexene: 3. Gas-phase and liquid-phase reaction on supported palladium, *Journal of Catalysis*, 52 (1978) 462-471.
- [3] R.J. Madon, E. Iglesia, Catalytic reaction rates in thermodynamically non-ideal systems, *Journal of Molecular Catalysis A: Chemical*, 163 (2000) 189-204.

- [4] M. Boudart, G. Djéga-Mariadassou, Kinetics of heterogeneous catalytic reactions, Princeton University Press, 2014.
- [5] M. Boudart, From the century of the rate equation to the century of the rate constants: a revolution in catalytic kinetics and assisted catalyst design, *Catalysis letters*, 65 (2000) 1-3.
- [6] A.V. Bridgwater, Review of fast pyrolysis of biomass and product upgrading, *Biomass Bioenerg.*, 38 (2012) 68-94.
- [7] S. Mukherjee, M.A. Vannice, Solvent effects in liquid-phase reactions: I. Activity and selectivity during citral hydrogenation on Pt/SiO₂ and evaluation of mass transfer effects, *Journal of Catalysis*, 243 (2006) 108-130.
- [8] C. Reichardt, T. Welton, Solvents and solvent effects in organic chemistry, John Wiley & Sons, 2011.
- [9] G. Li, B. Wang, D.E. Resasco, Water-mediated heterogeneously catalyzed reactions, *ACS Catalysis*, 10 (2019) 1294-1309.
- [10] D.E. Resasco, B. Wang, D. Sabatini, Distributed processes for biomass conversion could aid UN Sustainable Development Goals, *Nature Catalysis*, 1 (2018) 731-735.
- [11] D.E. Resasco, Carbon nanohybrids used as catalysts and emulsifiers for reactions in biphasic aqueous/organic systems, *Chinese Journal of Catalysis*, 35 (2014) 798-806.
- [12] D.E. Resasco, B. Wang, S. Crossley, Zeolite-catalysed C–C bond forming reactions for biomass conversion to fuels and chemicals, *Catalysis Science & Technology*, 6 (2016) 2543-2559.
- [13] E. Toukoniitty, P. Mäki-Arvela, J. Kuusisto, V. Nieminen, J. Päivärinta, M. Hotokka, T. Salmi, D.Y. Murzin, Solvent effects in enantioselective hydrogenation of 1-phenyl-1, 2-propanedione, *Journal of Molecular Catalysis A: Chemical*, 192 (2003) 135-151.
- [14] N.M. Bertero, A.F. Trasarti, C.R. Apesteguía, A.J. Marchi, Solvent effect in the liquid-phase hydrogenation of acetophenone over Ni/SiO₂: a comprehensive study of the phenomenon, *Applied Catalysis A: General*, 394 (2011) 228-238.
- [15] M.J. Vaidya, S.M. Kulkarni, R.V. Chaudhari, Synthesis of p-aminophenol by catalytic hydrogenation of p-nitrophenol, *Organic process research & development*, 7 (2003) 202-208.
- [16] H. Lo, M. Paulaitis, Estimation of solvent effects on chemical reaction rates using UNIFAC group contribution, *AIChE Journal*, 27 (1981) 842-844.
- [17] R. Rajadhyaksha, S. Karwa, Solvent effects in catalytic hydrogenation, *Chemical engineering science*, 41 (1986) 1765-1770.
- [18] U.K. Singh, M.A. Vannice, Kinetics of liquid-phase hydrogenation reactions over supported metal catalysts—a review, *Applied Catalysis A: General*, 213 (2001) 1-24.
- [19] R.J. Madon, E. Iglesia, Catalytic reaction rates in thermodynamically non-ideal systems, *Journal of Molecular Catalysis A: Chemical*, 163 (2000) 189-204.
- [20] G. Li, B. Wang D. E. Resasco, Solvent Effects on Catalytic Reactions and Related Phenomena at Liquid-Solid Interfaces, unpublished.
- [21] D.T. Bregante, A.M. Johnson, A.Y. Patel, E.Z. Ayla, M.J. Cordon, B.C. Bukowski, J. Greeley, R. Gounder, D.W. Flaherty, Cooperative Effects between Hydrophilic Pores and Solvents: Catalytic Consequences of Hydrogen Bonding on Alkene Epoxidation in Zeolites, *Journal of the American Chemical Society*, 141 (2019) 7302-7319.
- [22] T. Schwartz, J. Bond, A thermodynamic and kinetic analysis of solvent-enhanced selectivity in monophasic and biphasic reactor systems, *Chemical Communications*, 53 (2017) 8148-8151.

- [23] T.J. Schwartz, T.S. Wesley, J.A. Dumesic, Modifying the Surface Properties of Heterogeneous Catalysts Using Polymer-Derived Microenvironments, *Topics in Catalysis*, 59 (2016) 19-28.
- [24] R.L. Augustine, P. Techasauvapak, Heterogeneous catalysis in organic synthesis. Part 9. Specific site solvent effects in catalytic hydrogenations, *Journal of molecular catalysis*, 87 (1994) 95-105.
- [25] S. Mukherjee, M.A. Vannice, Solvent effects in liquid-phase reactions II. Kinetic modeling for citral hydrogenation, *Journal of Catalysis*, 243 (2006) 131-148.
- [26] D.D. Hibbitts, B.T. Loveless, M. Neurock, E. Iglesia, Mechanistic role of water on the rate and selectivity of Fischer–Tropsch synthesis on ruthenium catalysts, *Angewandte Chemie International Edition*, 52 (2013) 12273-12278.
- [27] B. Akpa, C. D’Agostino, L. Gladden, K. Hindle, H. Manyar, J. McGregor, R. Li, M. Neurock, N. Sinha, E. Stitt, Solvent effects in the hydrogenation of 2-butanone, *Journal of catalysis*, 289 (2012) 30-41.
- [28] M. Hronec, K. Fulajtarová, T. Liptaj, Effect of catalyst and solvent on the furan ring rearrangement to cyclopentanone, *Applied Catalysis A: General*, 437 (2012) 104-111.
- [29] G. Li, B. Wang, D.E. Resasco, Water Promotion (or Inhibition) of Condensation Reactions Depends on Exposed Cerium Oxide Catalyst Facets, *ACS Catalysis*, 10 (2020) 5373-5382.
- [30] F. Anaya, D.E. Resasco, Enhanced Fischer–Tropsch Synthesis Rates by the Combined Presence of Aqueous and Organic Media in Biphasic Systems, *ACS Catalysis*, 10 (2020) 4433-4443.
- [31] G. Li, B. Wang, B. Chen, D.E. Resasco, Role of water in cyclopentanone self-condensation reaction catalyzed by MCM-41 functionalized with sulfonic acid groups, *J Catal*, 377 (2019) 245-254.
- [32] C.T. Campbell, J.R. Sellers, Enthalpies and entropies of adsorption on well-defined oxide surfaces: Experimental measurements, *Chemical reviews*, 113 (2013) 4106-4135.
- [33] N. Singh, C.T. Campbell, A simple bond-additivity model explains large decreases in heats of adsorption in solvents versus gas phase: a case study with phenol on Pt (111) in water, *ACS Catalysis*, 9 (2019) 8116-8127.
- [34] T. Balankura, X. Qi, K.A. Fichthorn, Solvent Effects on Molecular Adsorption on Ag Surfaces: Polyvinylpyrrolidone Oligomers, *The Journal of Physical Chemistry C*, 122 (2018) 14566-14573.
- [35] H. Wan, A. Vitter, R.V. Chaudhari, B. Subramaniam, Kinetic investigations of unusual solvent effects during Ru/C catalyzed hydrogenation of model oxygenates, *Journal of catalysis*, 309 (2014) 174-184.
- [36] N.S. Gould, B. Xu, Catalyst characterization in the presence of solvent: development of liquid phase structure–activity relationships, *Chemical science*, 9 (2018) 281-287.
- [37] S. Wilkinson, I. McManus, H. Daly, J. Thompson, C. Hardacre, N.S. Bonab, J. Ten Dam, M. Simmons, C. D’Agostino, J. McGregor, A kinetic analysis methodology to elucidate the roles of metal, support and solvent for the hydrogenation of 4-phenyl-2-butanone over Pt/TiO₂, *Journal of Catalysis*, 330 (2015) 362-373.
- [38] D.Y. Murzin, Solvent effects in catalysis: implementation for modelling of kinetics, *Catalysis Science & Technology*, 6 (2016) 5700-5713.
- [39] M. Saeys, M.-F. Reyniers, J.W. Thybaut, M. Neurock, G.B. Marin, First-principles based kinetic model for the hydrogenation of toluene, *Journal of Catalysis*, 236 (2005) 129-138.

- [40] G. Bergeret, P. Gallezot, Particle size and dispersion measurements, Handbook of heterogeneous catalysis, (2008).
- [41] A.L. Denning, H. Dang, Z. Liu, K.M. Nicholas, F.C. Jentoft, Deoxydehydration of Glycols Catalyzed by Carbon- Supported Perrhenate, ChemCatChem, 5 (2013) 3567-3570.
- [42] V.K. Diez, C.R. Apesteguía, J.I. Di Cosimo, Aldol condensation of citral with acetone on MgO and alkali-promoted MgO catalysts, Journal of Catalysis, 240 (2006) 235-244.
- [43] J. Zelin, A.F. Trasarti, C.R. Apesteguía, Self-metathesis of methyl oleate on silica-supported Hoveyda–Grubbs catalysts, Catalysis Communications, 42 (2013) 84-88.
- [44] R.M. Silverstein, F.X. Webster, D.J. Kiemle, D.L. Bryce, Spectrometric identification of organic compounds, John Wiley & sons, 2014.
- [45] S. Sitthisa, D.E. Resasco, Hydrodeoxygenation of furfural over supported metal catalysts: a comparative study of Cu, Pd and Ni, Catalysis letters, 141 (2011) 784-791.
- [46] G. Kresse, J. Furthmuller, Efficient Iterative Schemes for ab Initio Total-Energy Calculations Using a Plane-Wave Basis Set, Physical Review B, 54 (1996) 11169-11186.
- [47] J.P. Perdew, K. Burke, M. Ernzerhof, Generalized Gradient Approximation Made Simple, Physical Review B, 77 (1996) 3865-3868.
- [48] P.E. Blochl, Projector Augmented-Wave Method, Physical Review B, 50 (1994) 17953-17979.
- [49] S. Grimme, J. Antony, S. Ehrlich, H. Krieg, A consistent and accurate ab initio parametrization of density functional dispersion correction [DFT-D] for the 94 elements H-Pu, The Journal of Chemical Physics, 132 (2010) 154104.
- [50] Stefan Grimme, Stephan Ehrlich, L. Goerigk, Effect of the Damping Function in Dispersion Corrected Density Functional Theory, The Journal of Computational Chemistry, 32 (2011) 1456-1465.
- [51] G. Henkelman, H. Jónsson, A dimer method for finding saddle points on high dimensional potential surfaces using only first derivatives, The Journal of Chemical Physics, 111 (1999) 7010-7022.
- [52] G. Henkelman, B.P. Uberuaga, H. Jónsson, A climbing image nudged elastic band method for finding saddle points and minimum energy paths, The Journal of chemical physics, 113 (2000) 9901-9904.
- [53] T. Mitsui, M. Rose, E. Fomin, D. Ogletree, M. Salmeron, Dissociative hydrogen adsorption on palladium requires aggregates of three or more vacancies, Nature, 422 (2003) 705-707.
- [54] R.M. Watwe, R.D. Cortright, J.K. Nørskov, J.A. Dumesic, Theoretical studies of stability and reactivity of C₂ hydrocarbon species on Pt clusters, Pt (111), and Pt (211), The Journal of Physical Chemistry B, 104 (2000) 2299-2310.
- [55] W. Eberhardt, S.G. Louie, E. Plummer, Interaction of hydrogen with a Pd (111) surface, Physical Review B, 28 (1983) 465.
- [56] G.W. Watson, R.P. Wells, D.J. Willock, G.J. Hutchings, A comparison of the adsorption and diffusion of hydrogen on the {111} surfaces of Ni, Pd, and Pt from density functional theory calculations, The Journal of Physical Chemistry B, 105 (2001) 4889-4894.
- [57] R.S. Rao, R.T.K. Baker, M.A. Vannice, Furfural hydrogenation over carbon- supported copper, Catalysis Letters, 60 (1999) 51-57.
- [58] L. Nie, D.E. Resasco, Kinetics and mechanism of m-cresol hydrodeoxygenation on a Pt/SiO₂ catalyst, Journal of Catalysis, 317 (2014) 22-29.

- [59] F. Cazaña, M. Jimaré, E. Romeo, V. Sebastián, S. Irusta, N. Latorre, C. Royo, A. Monzón, Kinetics of liquid phase cyclohexene hydrogenation on Pd–Al/biomorphic carbon catalysts, *Catalysis Today*, 249 (2015) 127-136.
- [60] J.K. Norskov, C.H. Christensen, Toward efficient hydrogen production at surfaces, *Science*, 312 (2006) 1322-1323.
- [61] D.S. Abrams, J.M. Prausnitz, Statistical thermodynamics of liquid mixtures: a new expression for the excess Gibbs energy of partly or completely miscible systems, *AIChE Journal*, 21 (1975) 116-128.
- [62] J. Rawlings, J. Ekerdt, *Chemical Reactor Analysis and Design Fundamentals*; Nob Hill Pub, LLC.: Madison WS, USA, 2002, Google Scholar.
- [63] K.J. Laidler, *Chemical kinetics*, 1987.
- [64] N. Singh, U. Sanyal, J.L. Fulton, O.Y. Gutiérrez, J.A. Lercher, C.T. Campbell, Quantifying Adsorption of Organic Molecules on Platinum in Aqueous Phase by Hydrogen Site Blocking and in Situ X-ray Absorption Spectroscopy, *ACS Catalysis*, 9 (2019) 6869-6881.
- [65] H. Ihm, H.M. Ajo, J. Gottfried, P. Bera, C.T. Campbell, Calorimetric measurement of the heat of adsorption of benzene on Pt (111), *The Journal of Physical Chemistry B*, 108 (2004) 14627-14633.
- [66] A.F. Lee, K. Wilson, R.M. Lambert, A. Goldoni, A. Baraldi, G. Paolucci, On the coverage-dependent adsorption geometry of benzene adsorbed on Pd {111}: a study by fast XPS and NEXAFS, *The Journal of Physical Chemistry B*, 104 (2000) 11729-11733.
- [67] M. Johansson, E. Skulason, G. Nielsen, S. Murphy, R.M. Nielsen, I. Chorkendorff, Hydrogen adsorption on palladium and palladium hydride at 1 bar, *Surface science*, 604 (2010) 718-729.
- [68] O. Haida, H. Suga, S. Seki, Calorimetric Study of the Glassy State. XI. Plural Glass Transition Phenomena of Cyclohexene, *Bulletin of the Chemical Society of Japan*, 50 (1977) 802-809.
- [69] J. Cox, D.D. Wagman, V.A. Medvedev, CODATA key values for thermodynamics, *Chem/Mats-Sci/E*, 1989.
- [70] I. Chorkendorff, J.W. Niemantsverdriet, *Concepts of modern catalysis and kinetics*, John Wiley & Sons, 2017.
- [71] M.A. Vannice, *Kinetics of catalytic reactions*, Springer, 2005.
- [72] C. Beckett, N. Freeman, K.S. Pitzer, The Thermodynamic Properties and Molecular Structure of Cyclopentene and Cyclohexene¹, *Journal of the American Chemical Society*, 70 (1948) 4227-4230.
- [73] L.H. Scharpen, J.E. Wollrab, D.P. Ames, Microwave spectrum, structure, and dipole moment of cyclohexene, *The Journal of Chemical Physics*, 49 (1968) 2368-2372.
- [74] J.F. Chiang, S.H. Bauer, Molecular structure of cyclohexene, *Journal of the American Chemical Society*, 91 (1969) 1898-1901.
- [75] J. Gates, L. Kesmodel, EELS analysis of the low temperature phase of ethylene chemisorbed on Pd (111), *Surface Science Letters*, 120 (1982) L461-L467.
- [76] C.T. Campbell, J.R. Sellers, The entropies of adsorbed molecules, *Journal of the American Chemical Society*, 134 (2012) 18109-18115.
- [77] J. Greeley, M. Mavrikakis, Surface and subsurface hydrogen: Adsorption properties on transition metals and near-surface alloys, *The Journal of Physical Chemistry B*, 109 (2005) 3460-3471.

- [78] M. Yamauchi, R. Ikeda, H. Kitagawa, M. Takata, Nanosize effects on hydrogen storage in palladium, *The Journal of Physical Chemistry C*, 112 (2008) 3294-3299.
- [79] M. Boudart, Two- step catalytic reactions, *AIChE Journal*, 18 (1972) 465-478.
- [80] S. Zhao, J. Cai, H. Chen, J. Shen, Understanding the effects of solvents on the hydrogenation of toluene over supported Pd and Ru catalysts, *Catalysis Communications*, 157 (2021) 106330.
- [81] H. Yook, K. Kim, J.H. Park, Y.-W. Suh, J.W. Han, Density functional theory study on the dehydrogenation of 1, 2-dimethyl cyclohexane and 2-methyl piperidine on Pd and Pt catalysts, *Catalysis Today*, 352 (2020) 345-353.
- [82] K. Kim, J. Oh, T.W. Kim, J.H. Park, J.W. Han, Y.-W. Suh, Different catalytic behaviors of Pd and Pt metals in decalin dehydrogenation to naphthalene, *Catalysis Science & Technology*, 7 (2017) 3728-3735.
- [83] A. Züttel, Materials for hydrogen storage, *Materials today*, 6 (2003) 24-33.
- [84] P. Chou, M.A. Vannice, Benzene hydrogenation over supported and unsupported palladium: II. Reaction model, *Journal of Catalysis*, 107 (1987) 140-153.
- [85] J.R. Elliott, C.T. Lira, *Introductory chemical engineering thermodynamics*, Prentice Hall PTR Upper Saddle River, NJ, 1999.
- [86] Z. Zhao, R. Bababrik, W. Xue, Y. Li, N.M. Briggs, D.-T. Nguyen, U. Nguyen, S.P. Crossley, S. Wang, B. Wang, D.E. Resasco, Solvent-mediated charge separation drives alternative hydrogenation path of furanics in liquid water, *Nature Catalysis*, 2 (2019) 431.
- [87] N. Pfriem, P.H. Hintermeier, S. Eckstein, S. Kim, Q. Liu, H. Shi, L. Milakovic, Y. Liu, G.L. Haller, E. Baráth, Role of the ionic environment in enhancing the activity of reacting molecules in zeolite pores, *Science*, 372 (2021) 952-957.
- [88] J. Shangguan, Y.-H.C. Chin, Kinetic significance of proton–electron transfer during condensed phase reduction of carbonyls on transition metal clusters, *ACS Catalysis*, 9 (2019) 1763-1778.
- [89] H. Cai, R. Schimmenti, H. Nie, M. Mavrikakis, Y.-H.C. Chin, Mechanistic Role of the Proton–Hydride Pair in Heteroarene Catalytic Hydrogenation, *ACS Catalysis*, 9 (2019) 9418-9437.